Universitat Autònoma de Barcelona

Departament de Química

Facultat de Ciències

New Functional Ligands for the Preparation of Photoactive Nanoparticle-Based Materials

Laura Amorín Ferré

Ph.D. Thesis

Ph.D. in Chemistry

2014

Supervisors:

Dr. José Luis Bourdelande Fernández

Dr. Félix Busqué Sánchez

Dr. Jordi Hernando Campos

III.2. RESULTS AND DISCUSSION

III.2.1. Synthesis and optical characterization of type I fluorescent ligands

To start with, we undertook the synthesis of type **I** fluorescent ligands, which are composed of a benzophenoxazine fluorophore and an unprotected *t*-butylcatechol moiety. Three different of these molecules were designed (**4**-**6**, Figure III-9), with which we wanted to explore: (a) different strategies for the attachment of the two functional units together (urea, in the case of **4**, and imino groups, in the case of **5** and **6**), and (b) the effects on the optical properties of the fluorescent group caused by the introduction of distinct electro-donating and electro-withdrawing substituents. After carrying out the synthesis of these ligands and studying their optical behavior, the best candidate for our next purposes would be chosen and a type **II** fluorescent molecule with an analogous structure would be finally prepared.

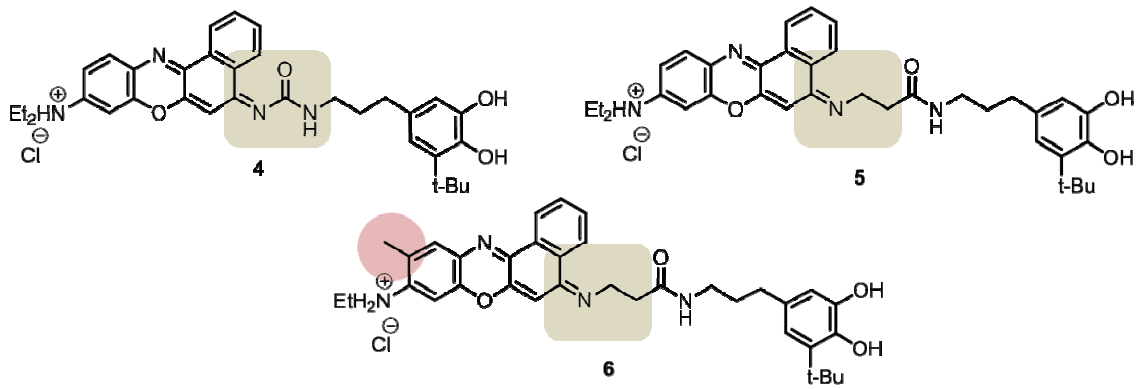

Figure III-9. Type **I** fluorescent ligands designed in this work. The structural differences between these molecules are highlighted in the figure.

Scheme III-1 shows the synthetic routes devised for the preparation of target compounds **4**-**6**, which were planned to be divergent from common catechol precursor **7** (see section III.2.1.1.). The formation of **4** would be accomplished by conversion of the amino group of **7** into an isocyanate moiety, followed by addition of the commercial benzophenoxazine dye nile blue A, **8**, and deprotection of the catechol unit. A different methodology would be used for the introduction of the fluorescent group into **7** for the synthesis of ligands **5** and **6**. In this case, the fluorophore would be prepared *in situ* by, first, tethering of an aminonaphtalene derivative to **7** and, second, subsequent reaction with nitrosophenols **9** and **10**, which would further lead to catechol deprotection and therefore directly furnish target compounds **5** and **6**, respectively.

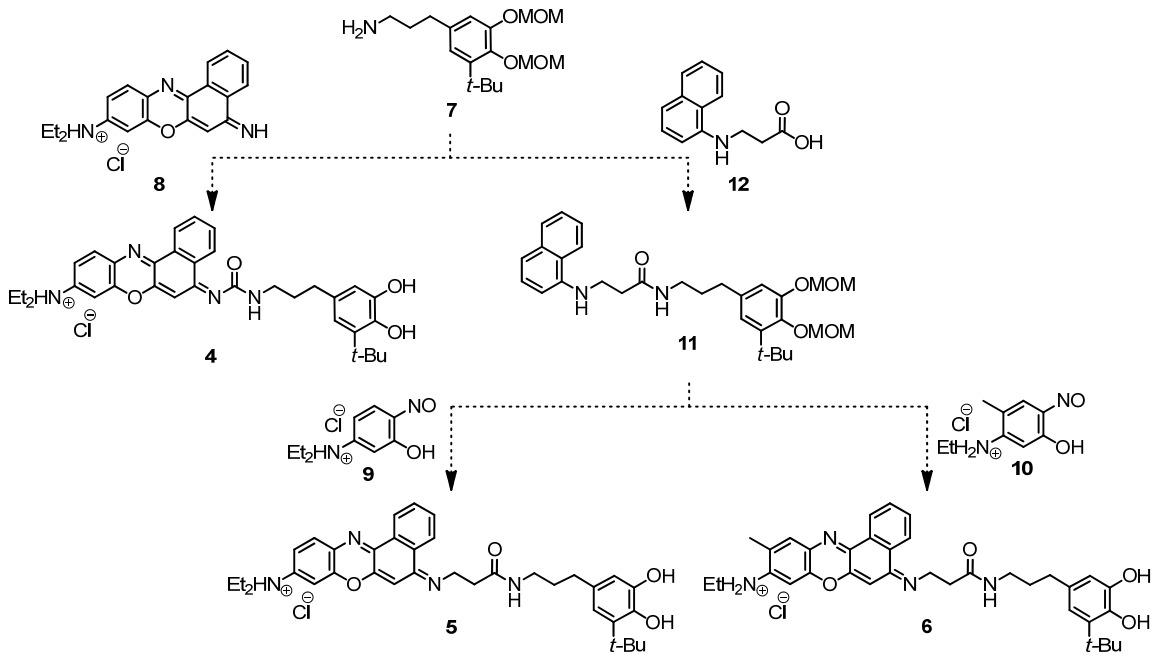

Scheme III-1. Synthetic routes designed in this work for the preparation of type **I** ligands **4**-**6**. In all cases, the catechol moiety of the final ligand would be introduced via the common intermediate **7**, whose synthesis is described in the next section.

III.2.1.1. Synthesis of intermediate 7

Scheme III-2 shows the route designed for the preparation of compound **7**, which starts from commercial 2-methoxy-4-methylphenol, **13**. Firstly, the aromatic electrophilic substitution at the 5-position of **13** followed by oxidation of the benzylic position and deprotection of the alcohol group lead to intermediate **14**. Next, protection of the catechol moiety as methoxymethyl ether (MOM) is chosen due to the mild conditions needed for cleaving it. The introduction of the nitrogenated functional group to obtain the desired intermediate **7**, has been envisioned by performing an aldol condensation followed by the reduction of the alkene and the nitrile group.

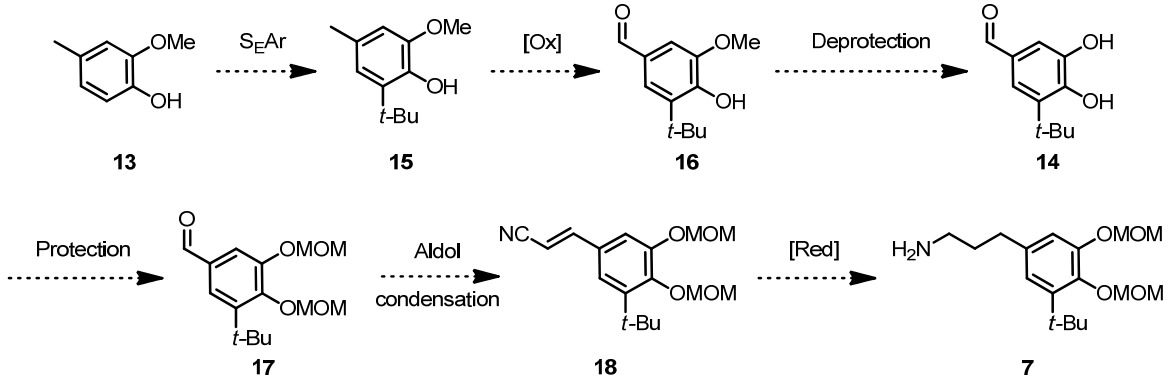

Scheme III-2. Synthetic route devised for the formation of intermediate **7**.

The first two steps of the synthesis of **7** had already been reported in the literature by Wang *et al.*, who described the preparation of compound **16** from **13**.[30] The same reaction conditions found in this report were directly applied in this work (Scheme III-3). Briefly, electrophilic aromatic substitution of **13** at 5-position was achieved by addition of *tert*-butanol in the presence of an excess of phosphoric acid, after which the benzylic position of the resulting intermediate **15** was oxidized with molecular bromine to yield **16**. These two steps were accomplished in agreement with the results described by Wang *et al.* (47 % overall yield for both steps).[30]

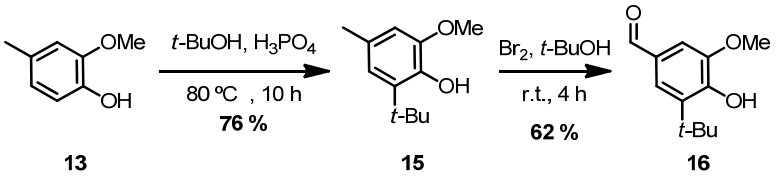

Scheme III-3. Synthetic procedure for the formation of compound **16** from commercial phenol **13** using the same conditions previously reported by Wang *et al.*[30]

Then, treatment of compound **16** with boron tribromide caused the cleavage of its methoxy group and the formation of catechol **14** with 90 % yield, as Bringmann *et al.* reported for a similar compound (Scheme III-4).[31] ^{1}H NMR showed the total disappearance of the proton signals corresponding to the methoxy group.

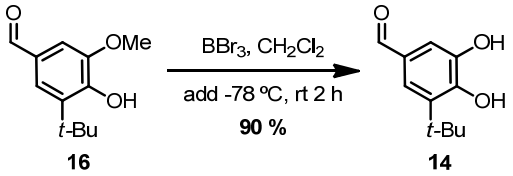

Scheme III-4. Hydroxyl deprotection reaction of **16** to yield catechol intermediate **14**.

In the next step, the hydroxyl moieties of the catechol intermediate **14** were converted into the corresponding methoxymethyl ethers, which are weak protecting groups whose cleavage takes place in catalytic acidic conditions.[32] These conditions are therefore to be avoided until the end of the synthesis of ligands **4**-**6**, as devised in Scheme III-1. Protection of the catechol moiety was achieved following a reported methodology.[33] The slow addition of methoxymethyl chloride to a solution of **14** under the conditions described in Scheme III-5 furnished compound **17** in quantitative yield after purification of the reaction crude by flash chromatography. ^{1}H NMR clearly showed the incorporation of the protecting groups owing to the occurrence of four new singlets corresponding to the methylene (at 5.31 and 5.23 ppm) and methyl protons (at 3.66 and 3.52 ppm) introduced.

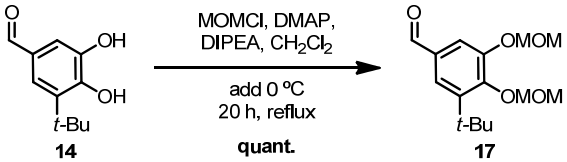

Scheme III-5. Reaction conditions used for the preparation of compound **17**.

The introduction into **17** of the nitrogenated group needed for the subsequent preparation of target compounds **4**-**6** could be accomplished by different routes. As described in Scheme III-6, Henry reaction with nitromethane and aldol condensation with acetonitrile were the simplest and less expensive strategies assayed for nitrogen incorporation; unfortunately, none of them succeeded in the formation of the new desired C-C bond for the obtaining of the corresponding nitro- and cianoderivatives, respectively. Alternatively, we explored the Wittig reaction with commercially available 2-(triphenylphosphoranylidene)acetonitrile, **19**, a stabilized phosphorane that reacted with the aldehyde moiety of **17** to furnish the target compound. After purification by flash chromatography, ^{1}H NMR analysis of the product showed the formation of (*Z*)- and (*E*)-**18** in 96 % yield and with a diasteromeric ratio of 2.3:1, respectively. Although this mixture could not be resolved by flash cromatography, its composition could be revealed on the basis of the different coupling constant values found between H-2 and H-3 in its ^{1}H NMR spectrum. According to the well-established NMR behavior for *trans* and *cis* olefinic protons,[34] the two doublets at 7.32 and 5.75 ppm with *J* = 16.6 Hz were assigned to (*E*)-**18**, while the two other doublets at 7.03 and 5.34 ppm with *J* = 12.2 Hz were attributed to the corresponding (*Z*)-isomer.

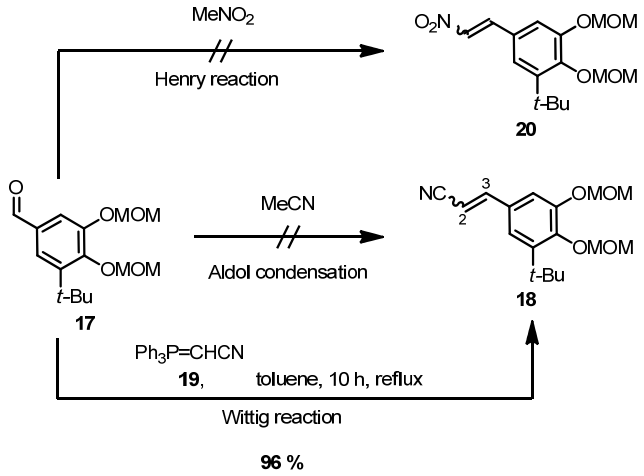

Scheme III-6. Different strategies assayed for the introduction of a nitrogenated group into intermediate **17**. Successful results were only obtained by means of Wittig reaction with **19**.

Next, we attempted hydrogenation of olefins (*E*)- and (*Z*)-**18** to convert this diastereomeric mixture into a single product. According to the literature,[35] when performing this reaction under palladium catalysis in the presence of proton donor solvents such as methanol, concomitant reduction of the nitrile moiety of **18** should occur, thus obtaining the desired amine **7** in a single step.

Nevertheless, analysis of the reaction crude by ^{1}H NMR when assaying these conditions showed only partial reduction of the nitrile group. For this reason, we decided to prepare **7** from **18** via a two-step process. As depicted in Scheme III-7, we first conducted selective reduction of the alkene moiety, which was achieved by using molecular hydrogen gas in the presence of Pd/C catalyst and in ethyl acetate medium. After product separation from the heterogeneous catalyst by simple filtration, this led to pure compound **21** in 68% yield. Next, this product was treated with lithium aluminum hydride in anhydrous diethyl ether to obtain compound **7** in 89% yield (60 % overall yield for both steps). ^{1}H NMR analysis of **7** showed the disappearance of the olefinic proton signals of compound **18** as well as the occurrence of three new signals for the alkyl protons arising from nitrile and alkene reduction: H-1 (at 2.73 ppm), H-2 (at 1.74 ppm) and H-3 (at 2.58 ppm), which were assigned on the basis of their multiplicity and of heteronuclear multiple bond correlation (HMBC) NMR experiments.

To summarize, compound **7**, the key common intermediate for the preparation of final target ligands **4**-**6**, was obtained in 7 reaction steps and in 24 % overall yield from the starting material 2-methoxy-4-methylphenol, **13**.

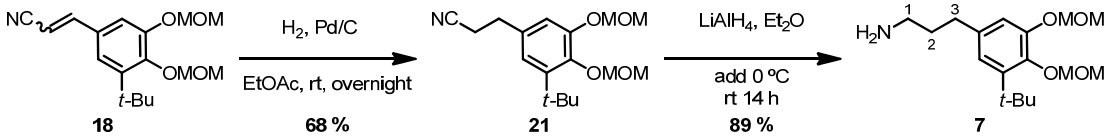

Scheme III-7. Reduction of alkene and nitrile moieties of compound **18** for the formation of intermediate **7**.

III.2.1.2. Synthesis of ligand 4

As previously described in Scheme III-1, the synthesis of fluorescent compound **4** was envisioned to take place from intermediate **7** through two additional reaction steps: (a) the introduction of the commercial benzophenoxazine dye nile blue A, **8**, by formation of an urea group, and (b) the cleavage of the MOM protecting groups.

The first step was designed on the basis of two previous independent works in which authors (i) converted the imino moiety of **8** into an urea by reaction between its conjugated base, **22**, and an isocyanate group,[36] and (ii) obtained an isocyanate group from an amine precursor by treatment with triphosgene.[37] In view of these reports, we first undertook the preparation of isocyanate **23** upon addition of triphosgene to a dichloromethane solution of **7** (Scheme III-8). When disappereance of the starting material was observed by TLC, **22** (prepared by treatment of commercial nile blue A with triethylamine) was directly poured to the mixture without any previous purification of the isocyanate intermediate. This led to a complicated reaction crude, which could not be resolved by flash chromatography. Instead, successive preparative TLCs were required to isolate urea **24** as a red crystalline solid in 5 % yield. Although the low amount obtained after the purification process did not allow complete characterization of **24** by ^{13}C NMR and IR, its formation was confirmed by ^{1}H NMR and HR-MS. In particular, new aromatic signals together with the

presence of a broad signal assigned to the -NH urea proton were observed in the ^{1}H NMR spectrum of this compound. Unfortunately, further attempts to improve the efficiency of the synthesis and separation of **24** were not successful and only very limited amounts of this compound could be obtained.

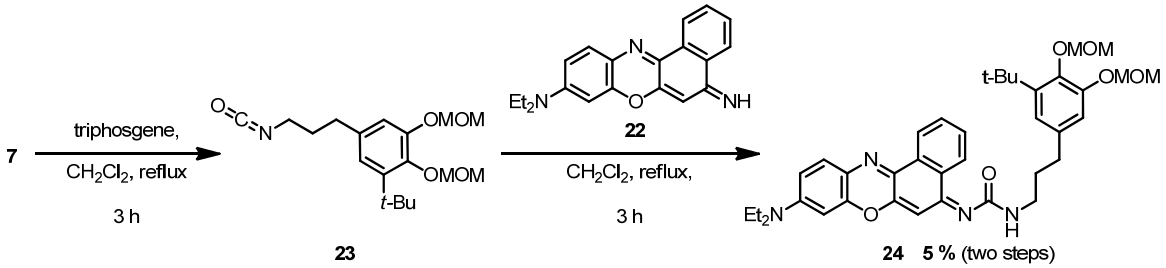

Scheme III-8. Consecutive reaction steps for the preparation of compound **24** from intermediate **7**, which consisted in the conversion of its amino group into an isocyanate followed by the introduction of the fluorophore by reaction with **22** and formation of a bridging urea group.

In spite of this, the preparation of target ligand **4** was pursued by exposing **24** to acidic conditions at reflux of methanol in order to deprotect its catechol moiety. In this way, fluorescent compound **4** was obtained in 40 % yield (Scheme III-9). The disappearance of the MOM signals in the ^{1}H NMR spectrum of this product demonstrated complete removal of the protecting groups, as subsequently confirmed by HR-MS. Further characterization of **4** by ^{13}C NMR and IR could not be carried out owing to the small scale at which this compound was obtained. Actually, the overall yield for the synthesis of **4** from commercially available 2-methoxy-4-methylphenol was just 0.5% after 10 reaction steps. This therefore dissuaded us to apply this ligand for the investigation of guest encapsulation and release from CPPs and, as a consequence, made us turn our attention to the synthesis of alternative type **I** ligands **5** and **6**.

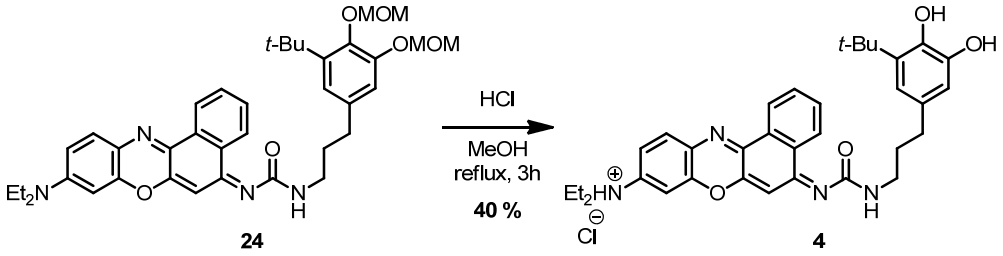

Scheme III-9. Reaction conditions for the formation of final target ligand **4**.

III.2.1.3. Synthesis of ligands 5 and 6

In contrast to compound **4**, the benzophenoxazine fluorescent unit of ligands **5** and **6** had to be prepared throughout our synthetic pathway following previous reports.[38] According to the route designed (see Scheme III.1), it involved two sequential steps: (a) introduction of a naphthalene moiety into intermediate **7** via amide formation by reaction with carboxylic acid **12**, and (b) subsequent coupling with nitrosophenol compounds **9** and **10**, which would lead to target products **5**

and **6**, respectively, by concomitant cleavage of catechol MOM protecting groups. It is important to remark that compounds **9**, **10** and **12** are not commercially available and their synthesis had to be carried out as described in the literature (Scheme III-10). Thus, compounds **9** and **10** were prepared by electrophilic aromatic substitution of commercial phenols **25** and **26** with sodium nitrite in similar yields to those reported by Martin-Brown *et al.*.[39] On the other hand, compound **12** was synthesized in 38% yield from commercial 1-naphthylamine, **27**, and 3-bromopropanoic acid, **28**, via nucleophilic substitution.[40] In all cases, the ^{1}H NMR spectra of the products obtained were in accordance with those previously described.

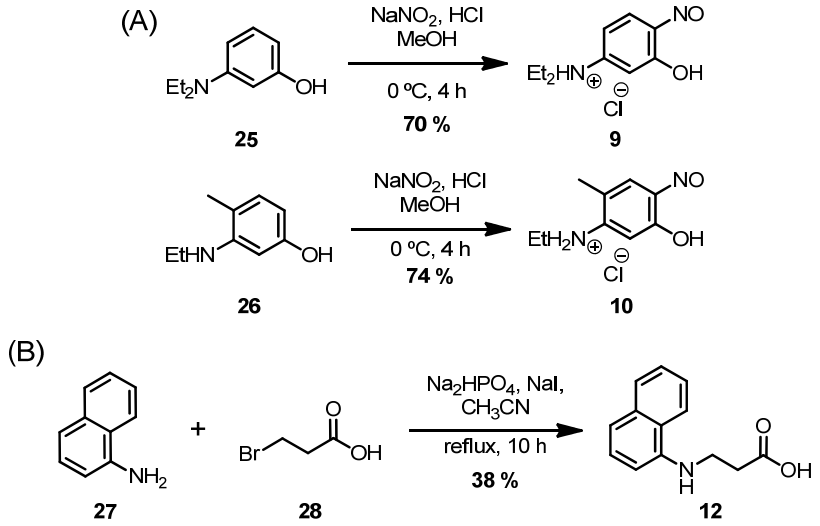

Scheme III-10. (A) Preparation of compounds **9** and **10** following the methodology described by Martin-Brown *et al*.[39] (B) Formation of compound **12** via nucleophilic substitution according to the procedure described by Frade *et al*.[40]

Once prepared naphthalene derivative **12**, it was reacted with intermediate **7** using typical amide formation conditions: *N*-ethyl-*N*'-(3-dimethyldiaminopropyl)-carbodiimide·HCl (EDCI) as coupling agent, hydroxybenzotriazole (HOBt) as additive and diisopropylethylamine (DIPEA) as base. In this way, compound **11** was obtained in 31 % yield (Scheme III-11). Nevertheless, no attempts of optimizing the reaction conditions were conducted since intermediate **7** was recovered after purification by flash chromatography and could be reused. The ^{1}H NMR spectrum of the purified product showed the combination of the proton signals of both consitutent units **7** and **12**, while the carboxylic ^{13}C NMR signal of **11** (171.9 ppm) was found to shift downfield with respect to **12** (164.4 ppm) described by Frade *et al*.[40] This confirmed the formation of the desired product **11**.

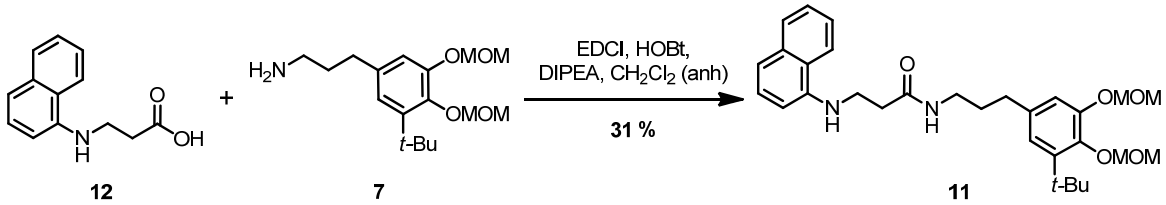

Scheme III-11. Reaction conditions for the coupling of **12** and **7** via amide bond formation.

This intermediate was then further reacted to yield the benzophenoxazine group of ligands **5** and **6** using the conditions reported by Frade *et al.* for the synthesis of analogous dyes.[40] With this aim, previously prepared nitrosophenol derivatives **9** or **10** were added over a solution of **10** with a catalytic amount of hydrogen chloride and subjected to reflux of methanol, thus furnishing the desired ligands **5** and **6** in 45 % and 35 % yield, respectively (Scheme III-12). Noticeably, the reaction conditions of this last step did not only allow the formation of the benzophenoxazine moiety, but also the cleavage of the MOM protective groups.[32] In contrast to **4**, both compounds could be simply purified by flash chromatography and fully characterized by ^{1}H NMR, ^{13}C NMR, IR and HR-MS. ^{1}H NMR showed the disappearance of the proton signals corresponding to the MOM protecting groups as well as distinct proton signals for (i) the conjugated π system of the benzophenoxazine moiety and (ii) the aromatic catechol group.

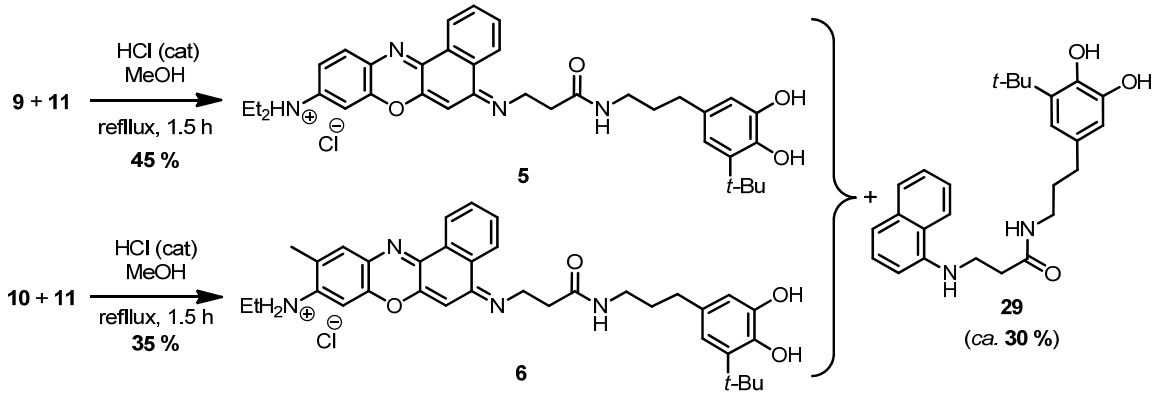

Scheme III-12. Last step of the synthetic procedure for the formation of target ligands **5** and **6**.

Despite achieving the successful preparation of **5** and **6**, the reaction yielded a major byproduct, which we identified as compound **29** by means of ^{1}H NMR analysis (Scheme III-12). Such product should arise from the cleavage of the MOM protecting groups of the starting material **11**. Evolution of **29** to fluorophore formation was not observed even when different reaction conditions were assayed (e.g. longer reaction times, higher concentration of hydrogen chloride or the addition of an excess of nitrosophenols **9** and **10**). However, analysis by ^{1}H NMR of the resulting reaction crudes only showed the formation of new undesired products and even lower yields for the synthesis of target compounds **5** and **6**. Despite this, the synthetic route to prepare ligands **5** and **6** and the easier purification procedures established allowed their preparation in a large enough scale as to attempt the subsequent synthesis of CPPs. In particular, target ligands **5** and **6** were both obtained in 9 steps and 3 % overall yield from commercial compound 2-methoxy-4-methylphenol, **13**.

III.2.1.4. Optical characterization of ligands 4, 5 and 6

The absorption and fluorescence spectra and the fluorescence quantum yields (Φ_{fl}) of the three ligands prepared were measured and analyzed using the commercial benzophenoxazine dye nile blue A, **8**, as a reference (Figure III-10 and Table III-1). In agreement with different reported works,

functionalization of the imino position of the benzophenoxazine group in **4**-**6** strongly affected the optical properties of the resulting fluorophores, which displayed clearly different spectra and Φ_{fl} values.[41] The most characteristic differences found were:

1. In all synthesized ligands, introduction of new groups at the imino position of the dye resulted in a clear decrease of their Stokes shift. This indicates the occurrence of more similar optimal geometries for the ground and first excited electronic states of compounds **4**-**6** with respect to nile blue A.
2. Functionalization of the imino group of the benzophenoxazine moiety as an urea in **4** resulted in three additional changes in optical properties with respect to nile blue A: (a) significant bathochromical shift of the absorption and emission spectra (*ca*. 20 nm, Table III-1); (b) more pronounced coupling between electronic and vibrational states, as demonstrated by the larger intensity of the 0→1 and 1→0 vibronic bands at λ=609 and 742 nm of the absorption and emission spectra of **4**, respectively; and (c) ~5-fold decrease of the fluorescence quantum yield (Table III-1) with respect to **8**.
3. In the case of ligands **5** and **6** ($\lambda_{max,Abs}$ = 620 nm, $\lambda_{max,Em}$ = 644 nm), alkylation of the imino group of the benzophenoxazine core also resulted in further variation of their optical behavior with respect to nile blue A. Thus, they displayed hypsochromic shift of their emission spectra (*ca*. 15 nm) and lower (for **5**) or higher (for **6**) fluorescence quantum yields (Table III-1). Nevertheless, it must be noticed that part of these differences, as well as those observed between both ligands prepared, must be ascribed to the distinct alkyl substituents introduced in other positions of the fluorophore group of **6** (see Figure III-9). In particular, removal of one ethyl group from the ammonium substituent of this compound and introduction of a methyl group at its relative *ortho* position clearly increased the Φ_{fl} value of **6** with respect to **5** and **8**, as already described by Frade *et al*. for analogous benzophenoxazine dyes.[40]

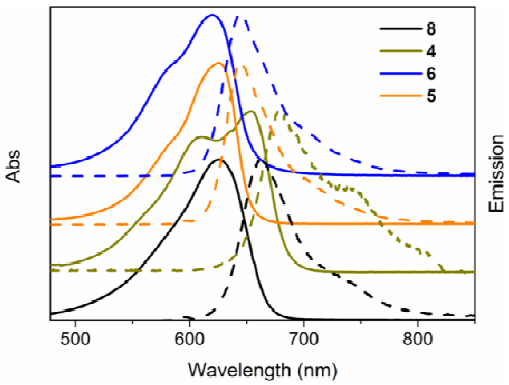

Figure III-10. Absorption (solid) and emission spectra (dash) of reference compound **8**, **4**, **5** and **6** in MeOH. All emission spectra were measured at λ_{exc} = 594 nm.

Table III-1. Optical properties of compounds **8**, **4**, **5** and **6**.

	$\lambda_{Abs,max}$ (nm)	$\lambda_{Em,max}$ (nm)	Stokes' shift (nm)	Φ_{fl}[a]
8	626	661	35	0.27[42]
4	653	678	25	0.05
5	626	644	18	0.13
6	620	644	24	0.40

[a]Determined in MeOH with **8** as a reference at λ_{exc} = 594 nm.

In view of these results and our previous synthetic studies, ligand **6** was selected as the best candidate for the subsequent preparation and investigation of guest-doped Co-based CPPs. Our choice was based on two different factors: (a) the higher yield achieved in the synthesis of **6** (and **5**) with respect to **4**; and (b) the larger fluorescent quantum yield measured for **6**.

III.2.2. Synthesis and optical characterization of type II fluorescent ligand

Once selected the type **I** ligand to be used in next stages of this work, we embarked ourselves in the synthesis of type **II** fluorescent compounds. To favor the comparative analysis of the results obtained in the encapsulation and release studies of these different species from CPPs, a single type **II** compound was designed, **30**, whose structure was nearly identical to that of the type **I** ligand **6** chosen (Figure III-11). The only difference between these two products lay in the functionalization of the hydroxyl groups of their catechol moiety, which in **30** were protected as methyl ethers to prevent its coordination to the metal ions of the CPPs to be formed. It must be noted that methyl ether groups are much more robust than the MOM protecting groups used along the synthesis of **6**, which should allow them to resist the acidic conditions required for the preparation of the final benzophenoxazine unit.

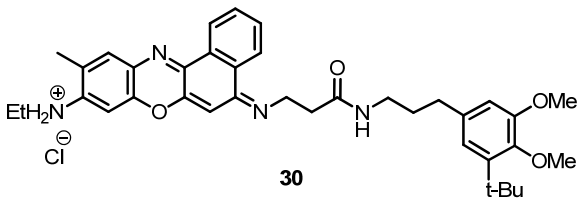

30

Figure III-11. Type **II** fluorescent compound to be prepared in this work, which was designed in analogy to type **I** ligand **6**.

The synthesis of **30** was designed according to the previous synthetic pathway developed for the formation of compound **6**. As shown in Scheme III-13, the protection of the synthesized intermediate **16** as methoxy group would lead to compound **31**, which contains the proper protecting

catechol group for the synthesis of the target ligand **30**. After performing the Wittig reaction between **31** and the phosphorane **19**, alkene and nitrile moieties of compound **32** would be reduced for the obtaining of amine **34**. Next, analogous procedure used for the formation of the benzophenoxazine group of ligand **5** would be carried out with compound **34** for the corresponding formation of **30**: firstly, the introduction of the aminonaphtalene derivative **12** to **34** via amide formation and, secondly, the reaction with the nitrosophenol compond **10**. Noticeably, none of the reaction conditions used would cause the cleavage of the methoxy groups, which need strong Lewis acids for their removal.

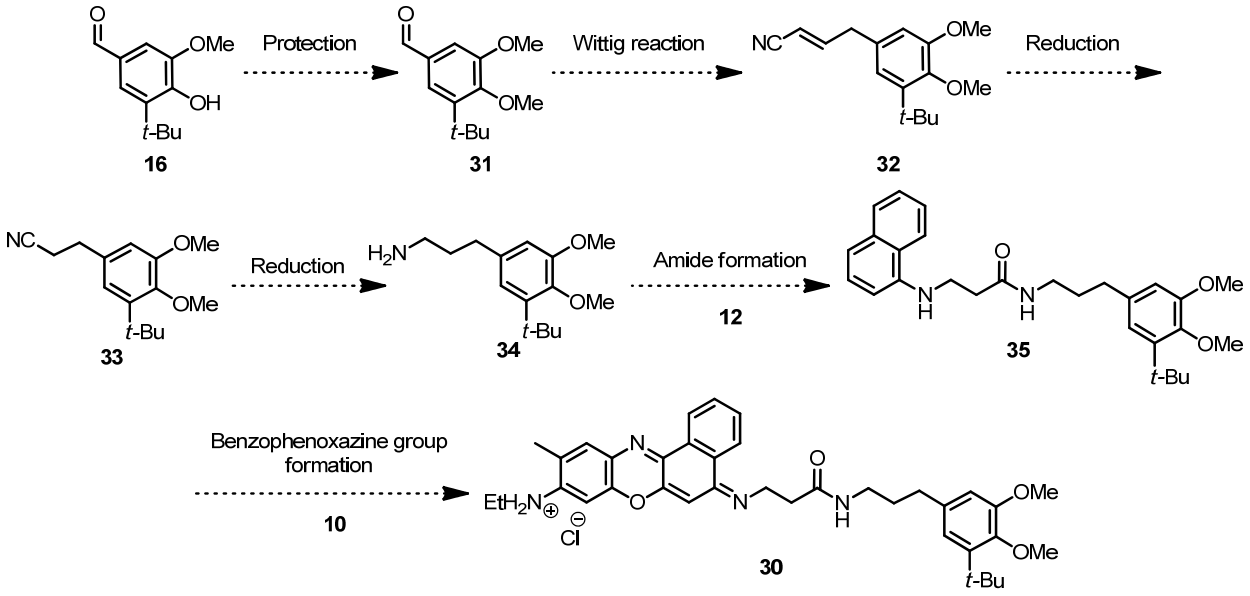

Scheme III-13. Synthetic route devised for the preparation of type **II** compound **30**.

The first step for the formation of **30** was the conversion of the free hydroxyl moiety of phenol **16** into a methyl ether protecting group. To achieve this, we applied the conditions previously described by Bringmann *et al.*, who carried out this reaction using dimethylsulfate as methylating agent.[31] In this way, compound **31** was obtained in 90% yield (Scheme III-14). ^{1}H NMR analysis of this product confirmed the successful protection of the starting material due to the appearance of a new singlet signal at 3.91 ppm for the methoxy group introduced.

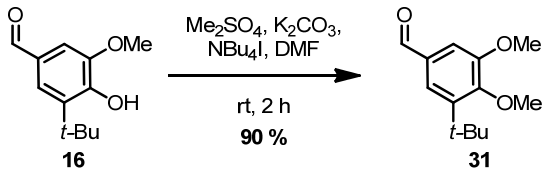

Scheme III-14. Synthetic conditions used for the formation of compound **31**.

Scheme III-15 summarizes the next reaction steps undertook, which were identical to those previously used for the formation of compound **6** from intermediate **17**. Thus, Wittig reaction

between 2-(triphenylphosphoranylidene)-acetonitrile and compound **31** yielded a diastereomeric mixture of (*E*)- and (Z)-**32** in 72 % yield and with a diastereomeric (*E*):(*Z*) ratio of 4.8:1 according to ^{1}H NMR data. This mixture was converted into single product **34** in 51% yield after consecutive reduction of their alkene and nitrile moieties using the same reaction conditions applied for the preparation of intermediate **7**. Indeed, the ^{1}H NMR spectra of compounds **34** and **7** exhibited very similar signals aside from those corresponding to their different hydroxyl protecting groups. The amino group of **34** was then reacted with carboxylic acid **12** to obtain amide **35** applying standard amide bond formation conditions. Finally, generation of the benzophenoxazine group was achieved by reaction between **35** and previously prepared nitrosophenol derivative **9** under acidic conditions, which yielded target type **II** compound **30** without cleavage of its methyl ether moieties. The ^{1}H and ^{13} C NMR spectra of this product were found to be nearly identical to those measured before for ligand **6**, although they additionally presented the signals arising from the methoxy protecting groups of **30**. In total, this product was obtained in 8 steps and 2% overall yield.

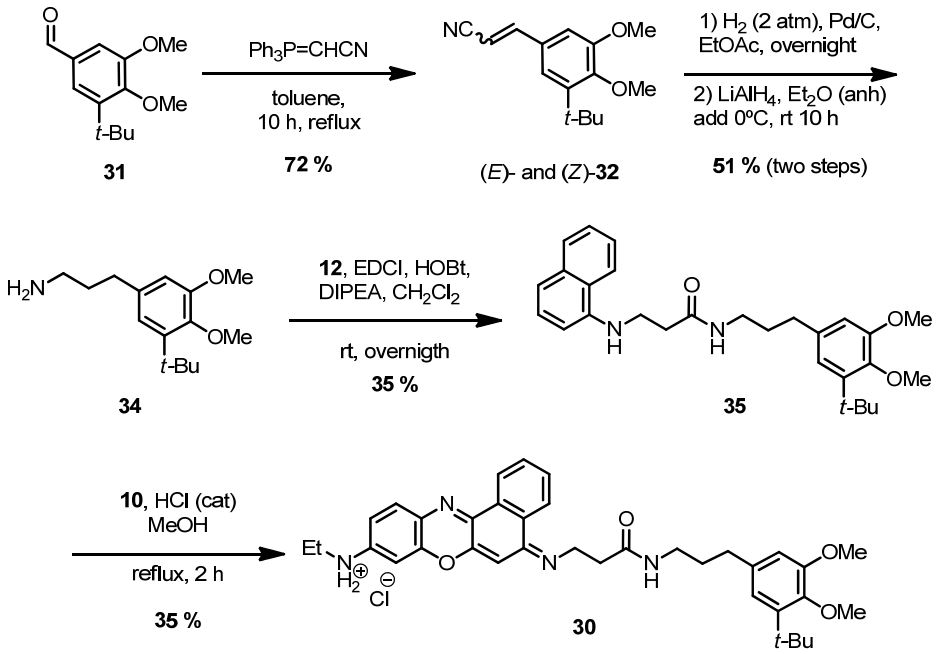

Scheme III-15. Synthetic methodology for the preparation of **30** followed in this work.

Once synthesized, the optical behavior of **30** was analyzed. Thus, its absorption and emission spectra and its fluorescence quantum yield were determined and compared to those of the analogous ligand **6** (Figure III-12 and Table III-2). Clearly, both compounds displayed nearly equivalent optical properties, as expected since they contain the same type of benzophenoxazine dye. In addition, this demonstrates that the catechol group of these products is fully electronically uncoupled from their fluorophore unit, and therefore, their optical spectra and Φ_{fl} values are completely independent of the protection state of the catecholic hydroxyl moieties.

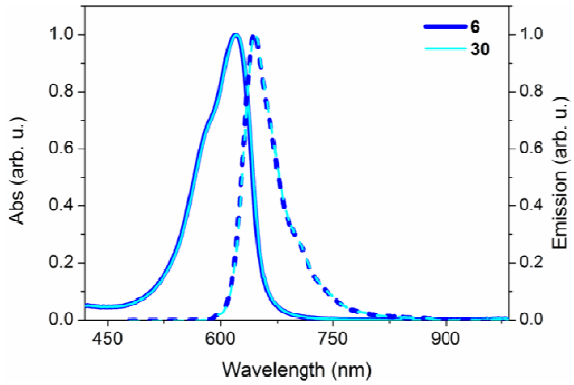

Figure III-12. Absorption (solid) and emission spectra (dash) of compounds **6** and **30** in MeOH (λ_{exc} = 594 nm).

Table III-2. Optical properties of **6** and **30** in methanol solution.

	$\lambda_{max,Abs}$ (nm)	$\lambda_{max,Em}$ (nm)	ε ($M^{-1}cm^{-1}$)	Φ_{fl}[a]
6	625	643	$4.8 \cdot 10^4$	0.40
30	626	645	$4.8 \cdot 10^4$	0.41

[a]Determined in MeOH with **8** as a reference at λ_{exc} = 594 nm.

III.2.3. Synthesis and characterization of CPPs

III.2.3.1. Synthesis and morphological characterization of CPPs

The incorporation of fluorescent compounds **6** and **30** into model CPPs for unraveling drug release mechanisms from these systems was done following a synthetic methodology already reported by Ruiz-Molina *et col*,[15] with whom this work was performed in collaboration. This strategy consisted in the use of cobalt acetate as the metal ion precursor, the bridging ligand **2** as linker and catechol **3** to complete the coordination sphere of the metal, which were converted into CPPs by means of the solvent-induced precipitation method (see section III.1.2). To these components, controlled amounts of **6** and **30** were added in our case to obtain the following materials: (a) Co-based CPPs doped with ligand **6** tethered to the coordination polymer, **M9**, and (b) Co-based CPPs with compound **30** lying physically entrapped, **M10**. In addition, same guest-free coordination

polymer particles were also prepared by means of the original procedure described by Ruiz-Molina *et col*,[15] **M5**, which were used as reference material in the characterization of **M9** and **M10**.

The first step towards the preparation of **M5**, **M9** and **M10** consisted in the synthesis of the bidentate organic linker **2**, which is not commercially available. The synthetic procedure described by Dhal *et al.* was applied,[43] which uses sodium hydride to form the conjugated base of commercial imidazole and thus enables nucleophilic substitution to the α,α'-dibromo-*p*-xylene substrate (Scheme III-16). In this way, the desired linker **2** was obtained in 55 % yield, characterized by ^{1}H NMR with results in agreement with previous spectral data,[43] and freshly used for the synthesis of CPPs.

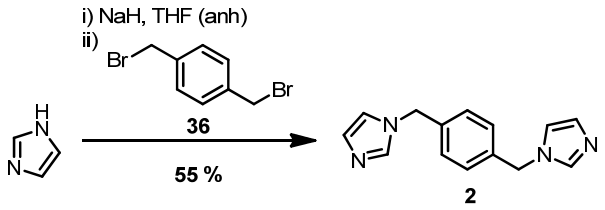

Scheme III-16. Procedure for the synthesis of bridging ligand **2**.

First CPPs formed were reference system **M5**, with which we aimed to implement in our group the synthetic methodology reported by Ruiz-Molina *et col.* (Figure III-13A). According to their procedure, the catechole and bisimidazole ligands **3** and **2** were dissolved in ethanol and an stoichometric ammount of an aqueous solution of cobalt acetate was added dropwise. A change of color (from pink to dark blue) occurred in approximately 10 min due to the oxidation process of the metal ion.[50] Subsequently, an excess of water (a poor solvent) was added to induce the precipitation of the CPPs, which were purified by consecutive centrifugation-redispersion cycles of the nanoparticles obtained in a mixture of ethanol:water (1:4). The resulting material was analyzed by SEM and TEM, which demonstrated the formation of solid nanoparticles with narrow size distribution and average diameter of (195 ± 38) nm (Figure III-13B-D). Furthermore, elemental analysis of these nanoparticles was consistent with the empiric formula $C_{32}H_{48}O_4CoN_2$. This result was in accordance to the previous reported by Imaz *et al.,*[15] whom described the coordination polymer particles as a network of coordination polymers consisted of units of one metal ion, one ligand **2**, and two molecules of **3**, where the metal ion mostly presented the *ls*-Co(III) valence (Co^{III}), ligand **2** (bix) acted as bridging ligand, and the coligand **3** presented two different forms in the same unit: (a) one catecholate form (3,5-dbcat) and (b) one semiquinonate form (3,5-dbsq). In this way, and accordingly to the results reported by Imaz *et al*., The monomeric formula of the CPPs synthesized in this work was defined as [Co^{III}(bix)(3,5-dbsq)(3,5-dbcat)].

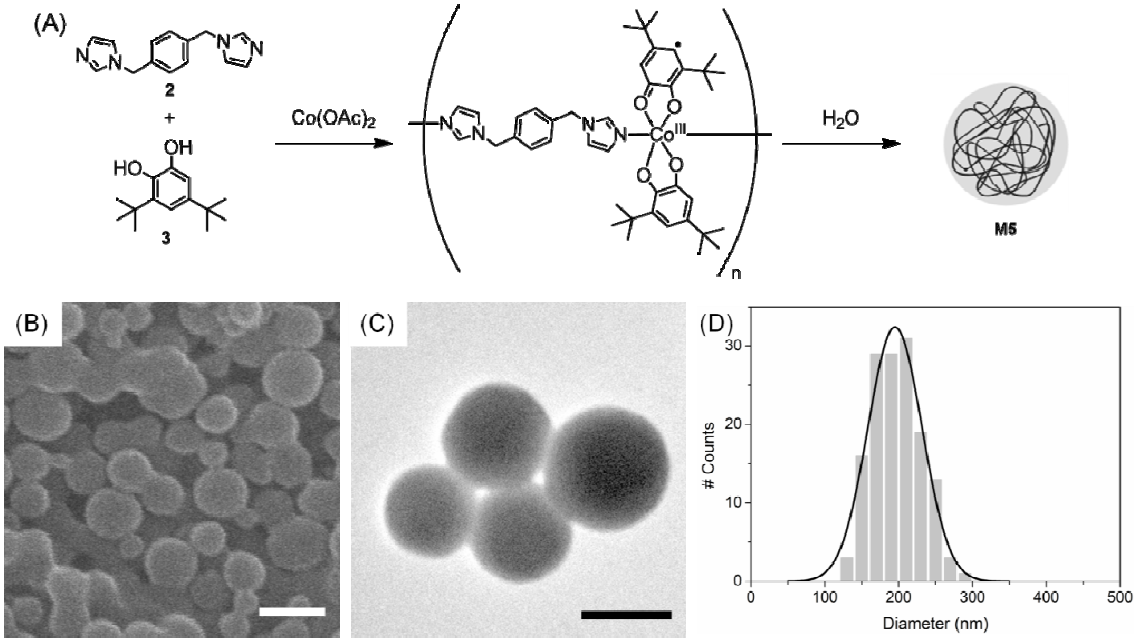

Figure III-13. (A) Synthesis of the guest free Co-based CPPs, **M5**. (B) SEM and (C) TEM images of the obtained **M5**. (D) Size histogram of the material determined from 150 nanoparticles.

Different results were obtained when applying the same procedure for the preparation of **M9**. In our first attempt, the unfunctionalized catechol **3** used in the synthesis of **M5** was fully replaced with ligand **6**, with which we intended to reach maximum encapsulation efficiency (i.e. two fluorescent guest molecules per each monomer of the coordination polymer formed, Figure III-14A). The resulting material (**M9a**) was analyzed by SEM. As shown in Figure III-14B, **M9a** consisted of two different populations of nano- and microsized particles with average diameters of (183 ± 32) nm and (1.13 ± 0.12) μm, respectively, even though equivalent reaction conditions to those used for the preparation of monodispersed **M5** CPPs had been applied. To further investigate this striking result, we first carried out SEM measurements of the **M9a** reaction mixture before adding the poor solvent. These experiments showed that the microparticles found in this material had already been generated prior to solvent-induced precipitation, together with the expected oligomeric structures of similar shapes and sizes to those reported by Mirkin *et col* for CPP formation.[10] We ascribed this behavior to the introduction of the benzophenoxazine fluorophore into the catechol group of **6**, which should decrease its solubility in the initial ethanol medium and lead to ligand aggregation into microparticles. To demonstrate this hypothesis, catechol ligands **6** and **29** were analyzed by SEM measurements (Figure III-14C and D). As expected, fluorophore-free catechol **29** did not self-structurate while catechol **6** did self-assemble into microsized particles, whose average diameter (1.39 ± 0.18 μm) was in agreement to that observed when synthesizing **M9a**. Such self-assembly process should be driven by π-π interactions between the benzophenoxazine groups in **6**, which prevented the formation of uniform doped Co-based CPPs. Instead, a mixture with microparticles solely formed by the fluorescent catechol ligand used was obtained. Unfortunately, attempts to remove such microparticles by treating **M9a** with an excess of ethanol turned to be unsuccessful,

which prompted us to develop a new strategy for the preparation of pure Co-based CPPs bearing fluorescent guest **6**.

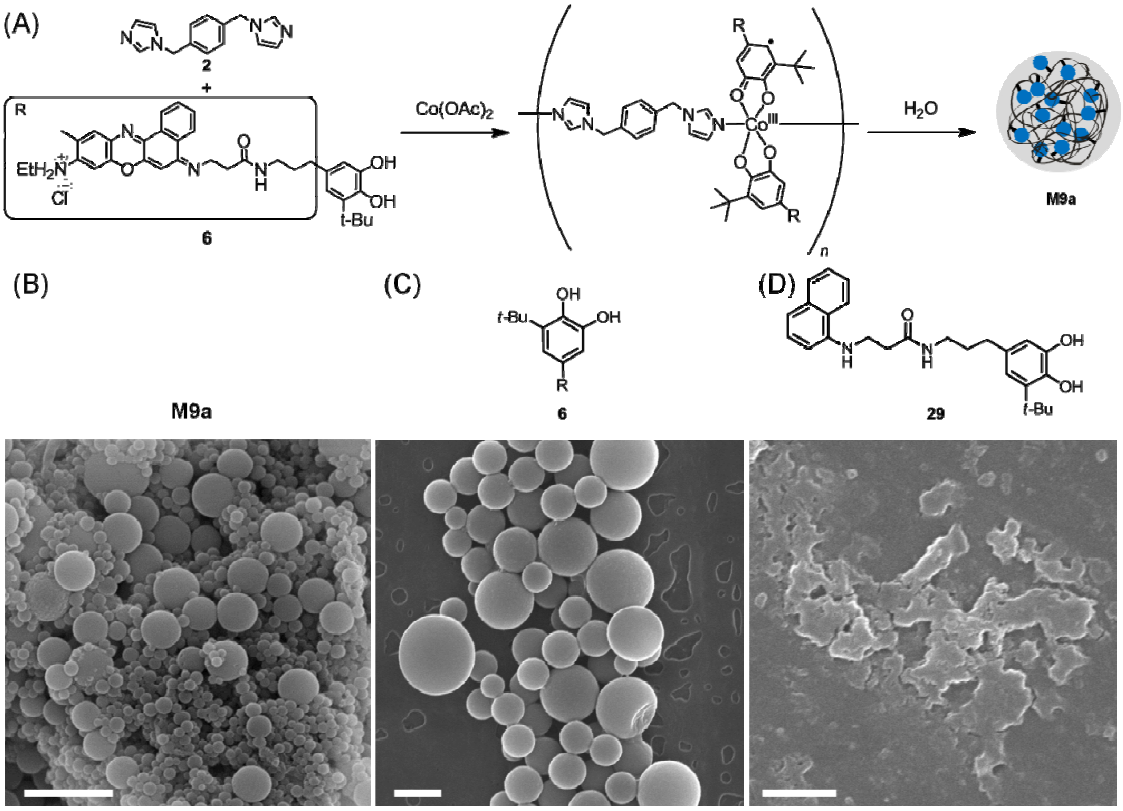

Figure III-14. (A) First reaction conditions assayed for the formation of **M9a**. SEM images of (B) the resulting **M9a** material, and (C) pure compound **6** and (D) pure compound **29**. Scale bars are 2 μm.

In particular, we considered diluting the amount of **6** used in the preparation of CPPs to avoid ligand self-assembly and self-structuration. For this reason, preliminary experiments were carried out where decreasing concentrations of **6** (20, 2, 0.2 and 0.02 mM) were treated with the CPP formation reaction conditions and the materials obtained after precipitation were analyzed by SEM to investigate self-structuration of the ligand. As shown in Figure III-15, spherical and even cube-shaped microparticles were obtained at concentrations higher than 1 mM. Instead, no ligand self-organization into defined microstructures was observed for the lowest concentration assayed, which was taken as a reference value for the next attempts of preparation of **M9**.

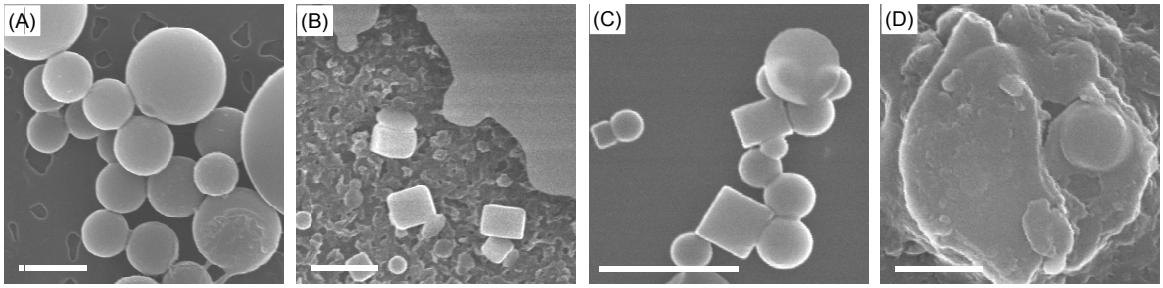

Figure III-15. SEM images of different concentrations of compound **6** of (A) 20 mM, (B) 2 mM, (C) 0.2 mM and (D) 0.02 mM. Scale bars are 2 μm.

Therefore, 0.02 mM concentrations of fluorescent guest **6** were used for the formation of the new material **M9b**, which should allow us to prevent self-aggregation of the ligand and therefore the formation of pure Co-based CPPs. It must be noted that this value accounted for only 1% of the total amount of catechol moieties required if the same concentrations of cobalt ions and bisimidazole linker **2** described by Ruiz-Molina *et col.*[15] and used for the preparation of **M5** had to be preserved. For this reason, 3,5-di-*tert*-buthylcatechol, **3**, was also added as co-ligand for the synthesis of **M9b**, and added in a ratio of 99:1 with respect to **6** in the reaction mixture (2.5 % wt content of **6**, Figure III-16A). In this way, the formation of monodispersed coordination polymer nanoparticles with average diameter of (152 ± 22) nm was achieved, as demonstrated by SEM and TEM measurements after sample purification by consecutive centrifugation-redispersion cycles in 1:4 ethanol:water mixtures (Figure III-16B-D). In addition, elemental analysis experiments showed good encapsulation efficiency since ligand **6** had been incorporated into the material that showed a molecular formula of $[Co^{III}(bix)(3,5\text{-}dbsq)_{0.92}(\mathbf{6})_{0.08}]$.

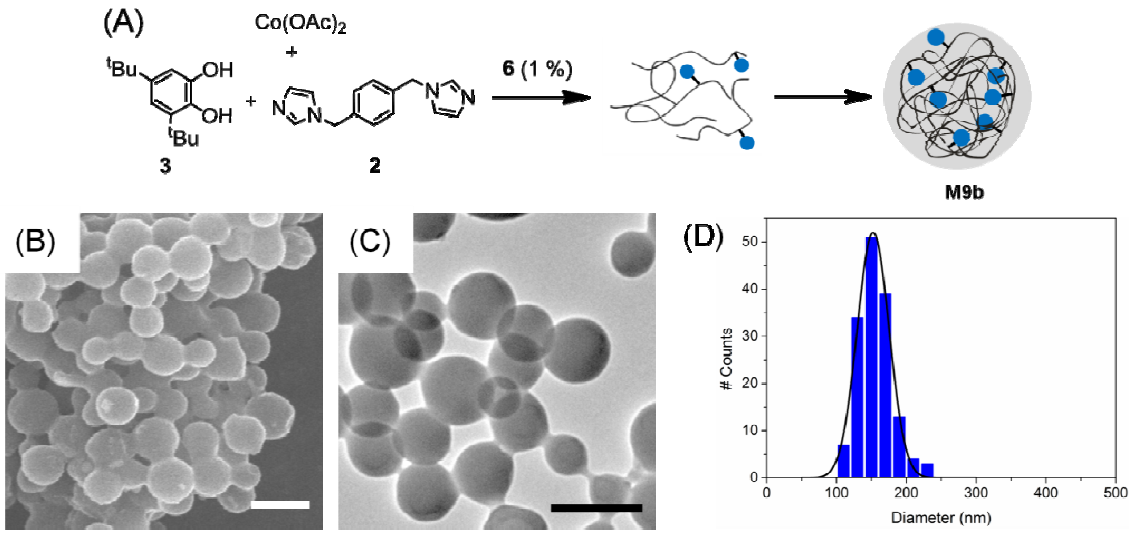

Figure III-16. (A) Schematic representation of the preparation of Co-based CPPs **M9b** doped with coordinating ligand **5**. (B) SEM and (C) TEM images of the resulting material; scale bar is 200 nm. (D) Size histogram determined from 150 nanoparticles.

In view of the good results obtained for **M9b**, Co-based CPPs bearing fluorescent guest **30** were prepared using equivalent conditions (i.e. 2.5 % wt of **30**). In this case, however, a stoichiometric amount of catechol ligand **3** was added, since the hydroxyl groups of **30** were protected and this compound could not coordinate cobat metal centers (Figure III-17A). After applying the same purification procedure as for **M9b**, the resulting material **M10** was analyzed by SEM and TEM (Figure III-17B-D). Clearly, nanometer-sized CPPs were successfully prepared with average diameter of (185 ± 37) nm. Elemental analysis results revealed an empiric formula of [Co^{III}(bix)(3,5-dbsq)(3,5-dbcat)] with 0.04 % wt of **30**.

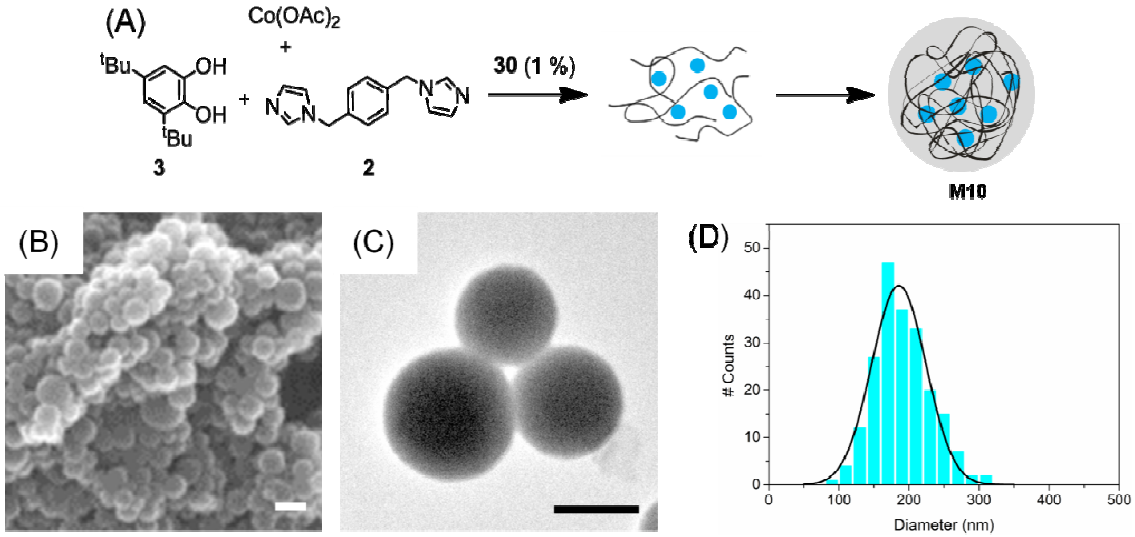

Figure III-17. (A) Schematic representation of the preparation of Co-based CPPs **M10** doped with non-coordinating ligand **30**. (B) SEM and (C) TEM images of the resulting material; scale bar is 200 nm. (D) Size histogram determined from 150 nanoparticles.

Noticeably, the morphology of target materials **M5**, **M9b** and **M10** was found to be very similar, since all of them consisted of full, spherical particles of nearly equivalent sizes. Probably, this came as an additional advantage of using very small amounts of the fluorescent guests **6** and **30** in the synthesis of CPPs **M9b** and **M10** (2.5 % wt), which made all three materials present very similar compositions. This is an important aspect to have in mind for future release studies from these particles, since the differences observed between them could be mainly attributed to the distinct encapsulation mechanisms of the guests instead of to different morphological features of the materials.

III.2.3.2. Magnetic and optical characterization of CPPs

X-ray diffraction could not be used to investigate the internal structure of **M5**, **M9b** and **M10** due to the amorphous nature of these materials. Instead, we exploited their valence tautomerism behavior to assess the structural similarities between them using magnetic measurements. Figure III-18 plots the thermal dependence of the effective magnetic moment (μ_{eff}) for the three CPPs

synthesized in this work. All three samples exhibited an abrupt change in μ_{eff} at approximately 300 K, which varied from μ_{eff} ~ 1.85 at 25 K to μ_{eff} > 3.0 at 380 K. As previously discussed by Ruiz-Molina *et col*. for a material analogous to **M5**,[15] this can be attributed to the interconversion from the *ls*-Co(III) (expected μ_{eff} = 1.76) to the *hs*-Co(II) (expected μ_{eff} = 5.08) tautomers of these materials.[18b] A thermally-induced electron transition from the cathecolate ligand to the Co(III) center of the low-spin state of the system accounts for this behavior, which results in metal ion reduction to Co(II) and ligand oxidation to its semiquinonate form. As such, the repeating unit of the coordination polymer network must become $[Co^{II}(bix)(3,5\text{-}dbsq)_2]_n$ after interconversion, although such process was not observed to be fully completed at the highest temperatures explored in our experiments since μ_{eff} values lower than 3.5 were recorded.

Importantly, thermal dependence of the magnetic moment and, therefore, valence tautomerism was not only shown by **M5**, but also by new materials **M9b** and **M10**. Clearly, this demonstrated that the introduction of 2.5 % wt. of fluorescent guests **6** and **30** into these CPPs did not affect the intrinsic valence tautomerism shown by Co-based coordination polymer particles composed of ligands **2** and **3**. Two main consequences can be derived from this observation that are relevant for our subsequent release studies: (a) the very similar μ_{eff} vs T curved registered for **M5**, **M9b** and **M10** indicate that these materials should be formed by equivalent coordination polymers in rather comparable phases, since both the occurrence of valence tautomerism and the actual range of temperatures at which the interconversion process takes place are extremely sensitive to the composition, structure and local environment of metal complexes;[18] (b) temperature might be exploited to modulate the delivery of the fluorescent guests from **M9b** and **M10**, since the electronic structures, geometries and chemical properties of these polymeric matrices should vary upon valence tautomeric interconversion.

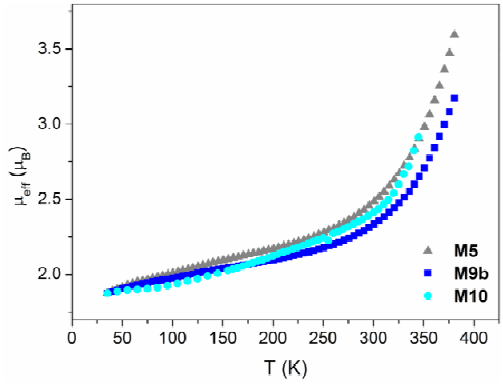

Figure III-18. μ_{eff} values as a function of temperature for **M5**, **M9b** and **M10** CPPs.

The optical properties of **M5**, **M9b** and **M10** were also investigated in detail. First, we used absorption measurements to determine the percentage of fluorescent guest molecules encapsulated within the CPPs, for which these particles had to be previously dissolved. As demonstrated by Spokoyny *et al.* for other metal-organic structures,[1] dissolution of **M5**, **M9b** and

M10 was observed upon addition of an organic solvent (methanol). When degassed methanol was used, the dispersed Co-based polymers were found to be fairly stable in solution, which allowed us registering their actual absorption spectra. As shown in Figure III-19A, guest-free **M5** treated in this way presented absorption bands at 400, 590 and 700 nm corresponding to intraligand, metal-to-ligand/ligand-to-metal charge transfer electronic transitions of the *ls*-Co(III) and *hs*-Co(II) repeating units of this material, respectively.[18b,44] Similar bands were observed when dissolving **M9b** and **M10** in degassed methanol, although the absorption spectra of these materials also showed an additional intense peak at 626 nm. According to the our previous measurements (see Figure III-12), this new band corresponds to the bezophenoxazine dye of the fluorescent guests **6** and **30** embedded into **M9b** and **M10**, respectively. Such a band was also found in the absorption spectra of **M9b** and **M10** dissolved in non-degassed methanol, as shown in Figure III-19B. However, the absorption bands corresponding to the Co-based coordination polymers of these materials and **M5** were observed to faint and a concomitant increase of a new peak at 400 nm was found at these conditions. We ascribed this behavior to polymer degradation under air atmosphere, which led to complete oxidation of its constituent catechol and semiquinone ligands into new quinone species with $\lambda_{max,Abs}$ ~ 400 nm.[45] This degradation process allowed the determination of the fluorescent dye cargo in both **M9b** and **M10** and, therefore, their encapsulation efficiency. Thus, 20 % of fluorescent catechol **6** initially added to the CPP formation medium was found to be tethered to **M9b**, while only 10% of the compound **30** used was measured to be entrapped into **M10**. Therefore, incorporation of the guest by coordination to the metal ion resulted in a more efficient encapsulation process than simple mechanical entrapment.

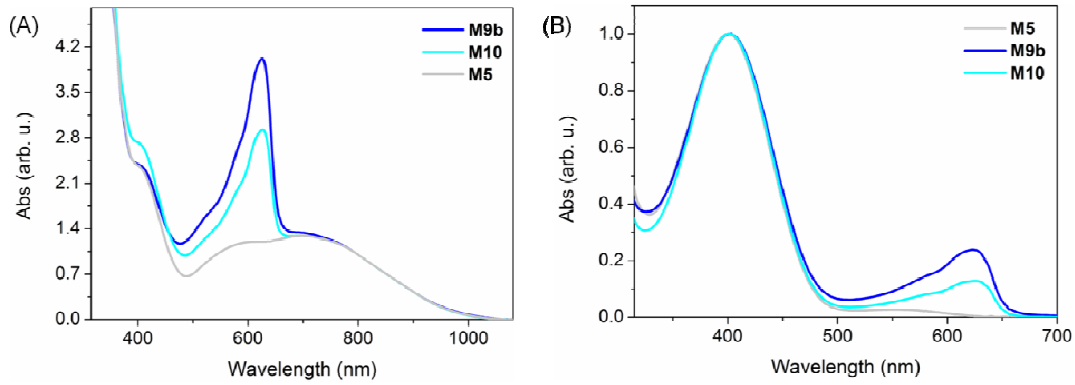

Figure III-19. Absorption spectra of **M5**, **M9b** and **M10** in (A) degassed MeOH and (B) non-degassed MeOH.

We also investigated the fluorescent properties of these materials both in the solid state and in solution. As already anticipated in our design of **M9b** and **M10**, none of these CPPs showed any emission in the solid state arising from the fluorescent guests **6** and **30** encapsulated This behavior was also observed upon dissolution of the particles with degassed methanol, which allowed preserving the structure of their constituent coordination polymers (Figure III-20A). Therefore, fluorescence quenching occurred in **M9b** and **M10**, which we ascribed to resonance energy transfer processes. RET is a non-radiative dipole-dipole mechanism through which electronic excitation

energy transfer can take place on the nanoscale from high excitation energy donors (in our case, benzophenoxazine fluorophores **6** and **30**, D) to lower excitation energy acceptors (the Co-based coordination polymers, A).[29] This makes the electronic excited state of the donors relax back to their ground state without emission of fluorescent photons, while the acceptors are promoted to their electronic excited state without direct absorption of the incoming excitation light. Since such acceptor species were not luminescent in our case, the overall result of the RET process in **M9b** and **M10** was fluorescence quenching of **6** and **30**.

The efficiency of resonance energy transfer processes depends on four main factors: (a) the spectral overlap between the absorption of A and the emission of D, which is large in our case due to the broad absorption spectrum spanning all over the visible and NIR regions of the Co-based coordination polymers used (Figure III-20B), (b) the Φ_{fl} value of the donor, which must be high; (c) the orientation between the absorption transition dipole of A and the emission transition dipole of D, since RET is a dipole-dipole energy transfer process; (d) the separation between donor and acceptor species, which must be lower or at least comparable to the Förster radius (R_0) defined as the D-A distance with 50 % probability of RET to occur. Actually, R_0 can be easily calculated for any D-A pair using Equation III-1,[29] where $\Phi_{fl,D}$ is the fluorescence quantum yield of D, κ is the geometrical factor that defines the orientation of the transition dipoles and J is the D-A spectral overlap integral. Using the values of $\Phi_{fl,D}$ and J determined from the optical properties measured for the separated donor and acceptor moieties in methanol ($\Phi_{fl,\mathbf{6}}$ = 0.40, $\Phi_{fl,\mathbf{30}}$ = 0.41, $J_{\mathbf{M9b}}$ = $1.24 \cdot 10^{-14}$, $J_{\mathbf{M10}}$ = $1.27 \cdot 10^{-14}$) and assuming random orientation between them (κ^2 = 2/3), R_0 was found to be on the nanometer scale both for **M9b** and **M10** ($R_{0,\mathbf{M9b}}$ = 4.70 and $R_{0,\mathbf{M10}}$ = 4.72). Taking into account Equation III-2 to predict the efficiency of the RET process (E_{RET}) from R_0 and the actual D-A distance ($r_{D\text{-}A}$),REF this means that $r_{D\text{-}A}$ must be lower than 2.19 nm to ensure complete fluorescence quenching (i.e. E_{RET} > 99 %) of **6** and **30** in **M9b** and **M10**, respectively. Such a requirement was fulfilled for sure in **M9b**, where the fluorescent guest **6** was expected to be directly tethered to the Co-based coordination polymer ($r_{D\text{-}A} \sim$ 1.68 nm). In case of **M10**, this indicates a close packing of the polymeric network, which should render the physically entrapped **30** molecules close enough to the energy acceptor coordination polymers.

$$R_0 = 9.78 \cdot 10^3 \sqrt[6]{\frac{\Phi_{fl,D} \cdot \kappa^2 \cdot J}{n^4}} \qquad \text{(III-1)}$$

$$E_{RET} = \frac{R_0^6}{R_0^6 + r^6} \qquad \text{(III-2)}$$

A further proof that RET accounted for the emission quenching of the fluorescent guests in **M9b** and **M10** was obtained by dissolving and degrading these materials by adding non-degassed

methanol. As previously discussed, this provoked the disappearance of the absorption bands in the red and NIR regions of the spectrum corresponding to the energy acceptor Co-based coordination polymers, thus precluding the spectral overlap with the emission of dyes **6** and **30** required for resonance energy transfer to take place (Figure III-20B). As a result, high fluorescence intensities were observed for both samples with $\lambda_{max,Em}$ = 645 nm, which arose from unquenched **6** and **30** molecules (Figure III-20A). This result was of relevance for our subsequent release studies, since it enabled selective detection of the guests delivered by means of fluorescence measurements. Thus, while no emission must be registered when they are coordinated, or close, to the coordination polymer network (i.e. when they are encapsulated), dyes **6** and **30** should turn fluorescent upon release. Therefore, all detected fluorescence could be taken as a direct measurement of the amount of delivered guests.

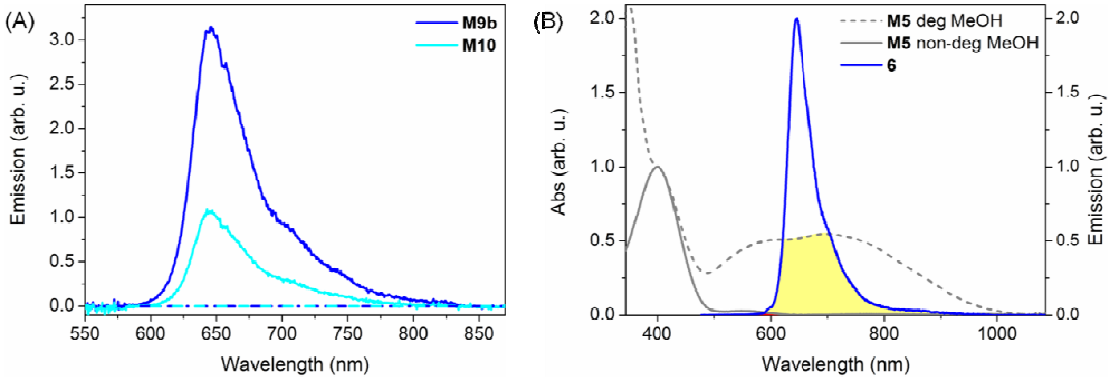

Figure III-20. (A) Fluorescence emission spectra recorded in degassed MeOH (dashed lines) and non-degassed MeOH (solid lines) for **M9b** and **M10**. (B) Spectra overlap (yellow area) between the absorption spectrum of **M5** in degassed MeOH and the fluorescence spectrum of compound **6** in MeOH. The absorption spectrum of **M5** after particle dissolution and coordination polymer degradation in non-degassed MeOH is also shown.

III.2.4. Guest release mechanisms

III.2.4.1. Guest release from M9b and M10 at physiological conditions

Once prepared and characterized, guest release experiments were carried out for **M9b** and **M10** at physiological conditions. In these experiments, a suspension of each material (**M9b** or **M10**) in PBS at pH = 7.4 was placed in a dialysis bag and dialyzed at 37 ºC for 100 hours. Small aliquots of the dialysate were then taken periodically in time and their emission registered to measure the relative cumulative release of fluorescent guests **6** and **30**. Absolute release efficiencies were finally determined by measuring the amount of fluorophore remaining in the solid within the dialysis bag at the end of the experiments by means of absorption measurements in non-degassed methanol. Figure III-21 plots the release profiles obtained in this way for **M9b** and **M10**. Clearly, high release

efficiencies were found for both materials after 100 hours of dialysis (*ca*. 90%). However, completely different profiles were measured, which should be attributed to the different encapsulation and release mechanisms expected for dyes **6** and **30** from **M9b** and **M10**, respectively. Thus, while it took approximately 10 h for 50% delivery of the fluorescent guest chemically tethered to **M9b**, a similar release efficiency was obtained for the mechanically entrapped molecules in **M10** in only 2 h. Taking into account that those materials were expected to display different delivery mechanisms, diffusion of physically encapsulated guests through the Co-based CPPs used should therefore take place in a shorter time scale than particle degradation, which is required for the release of chemically bonded molecules.

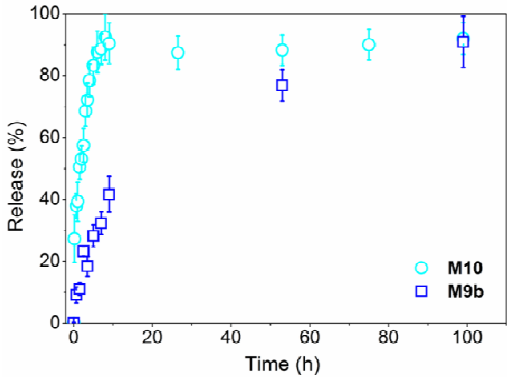

Figure III-21. Cumulative release profiles of fluorescent guest molecules **6** and **30** from **M9b** and **M10** in PBS at 37 ºC, respectively. Each data set was obtained after averaging over 4 independent experiments.

In view of this, we first focused on the analysis of the release of **30** from **M10**, which we assumed to proceed mainly via fast diffusion processes. There exist several theoretical models that describe diffusion-induced drug delivery, which have been mainly developed for organic polymeric nano- and microparticles.[46] In our case we considered the model shown in Equation III-3, where M_t and M_∞ are the cumulative absolute amounts of guest released at time t and infinity, R is the radius of the particles (185 nm) and k_D is the apparent diffusion constant of the drug within the system:.

$$M_t = M_\infty \cdot \left(1 - \frac{6}{\pi^2}\sum_{n=1}^{\infty}\frac{1}{n^2}\exp\left(-\frac{k_D n^2 \pi^2 t}{R^2}\right)\right) \qquad \text{(III-3)}$$

This model assumes Fickian's diffusion from spherical particles with homogeneous and low-doping loads of guests as in **M10**, which should not undergo any degradation during the release process. To verify whether the latter condition applied to our system, SEM images of the dialyzed particles were measured at 0, 5, 26 and 100 hours. As displayed in Figure III-22, surface erosion and particle degradation were observed after 26 hours in PBS at 37ºC. Nevertheless, no degradation effects were observed for the first 5 hours when nearly 84 % of the total guest release took place. Accordingly, Equation III-3 provided with a reasonable model to account for guest

delivery from **M10**. Actually, when fitting this equation to our experimental release data, a very good agreement was found and a k_D value of $6.9 \cdot 10^{-19}$ m^2 s^{-1} was retrieved (Figure III-23A). This allowed us to unambiguously identify diffusion of physically encapsulated molecules through the polymeric network of **M10** as the main release mechanism operating in this material.

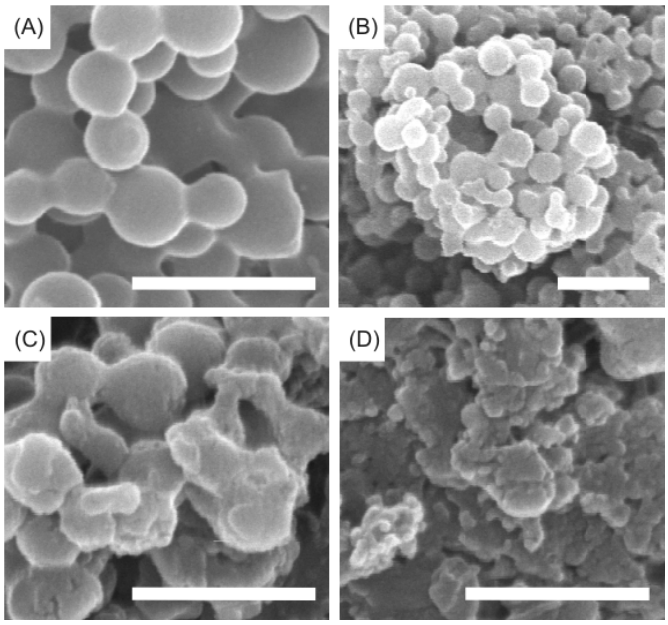

Figure III-22. SEM images of **M10** CPPs suspended at 37 ºC in PBS for (A) 0 h, (B) 5 h, (C) 26 h and (D) 100 h. Scale bars are 500 nm.

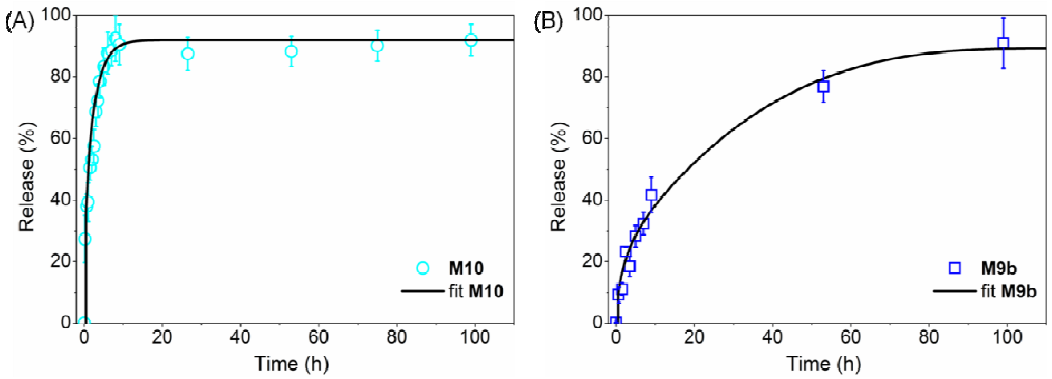

Figure III-23. Fitting curves (solid lines) of the experimental cumulative release profiles of (A) **M10** and (B) **M9b** according to the models given by equations III-3 and III-4.

Next, a similar mechanistic investigation of the release profile from **M9b** was undertaken. In a first step, single-mechanism degradation models such as surface degradation[47] or bulk erosion[48] were considered, since all encapsulated guests were expected to be chemically tethered to the material. However, poor agreement was found between these models and our experimental data. A plausible explanation for this could be that a non-negligible fraction of the encapsulated molecules were physically entrapped into these CPPs instead of covalently bonded. In this case, both diffusion

and degradation processes should induce guest release from **M9b**. This prompted us to develop Equation III-4, which was derived to account for the occurrence of these two mechanisms:

$$M_t = M_\infty \cdot \left(b\left(1 - \frac{6}{\pi^2}\sum_{n=1}^{\infty}\frac{1}{n^2}\exp\left(-\frac{k_D n^2 \pi^2 t}{R^2}\right)\right) + (1-b)\left(1-\left(1-\frac{k_d t}{(1-b)C_0 R}\right)^3\right)\right) \quad \text{(III-4)}$$

This equation consists of two different terms: (a) the first term corresponds to the diffusion-induced release of physically encapsulated guest fluorophores, which should follow the same Fickian model applied for **M10** (see Equation III-3); and (b) the second term is related to the Hopfenberg's model, an empirical surface-erosion equation developed for spherical particles that exhibit heterogeneous degradation.[49] Such a term, which should account for the delivery of chemically bonded molecules, depends on three different parameters: the surface erosion rate constant (k_d), the total initial concentration of the guest in the polymer matrix (C_0), and the initial radius of the nanoparticles (R). Moreover, an additional factor b was introduced, which is the fraction of guest molecules that lie mechanically entrapped within **M9b** and therefore reports on the contribution of each one of the terms in the equation to the overall release process. As both materials **M9b** and **M10** were expected to be morphologically equivalent and the molecular geometries of guests **6** and **30** very similar, the apparent diffusion constant for the first term in Equation III-4, k_D was assumed to be the same as that determined for **M10**. Thus, this equation was fitted to our experimental data using only two variable parameters, b and k_d. In spite of this, a good agreement was found, as demonstrated in Figure III-23B. Noticeably, a value of b = 0.26 was retrieved from the fit, which meant that 26 % of the encapsulated fluorescent guests were mechanically entrapped within the particles. The remaining 74 % of compound **6** was covalently linked to the polymer matrix of **M9b** and released via particle degradation with a slow rate constant ($k_d/C_0 = 3.31 \cdot 10^{-13}$ m s^{-1}). Therefore, both diffusion and degradation processes accounted for guest delivery from **M9b**, thus giving rise to a two-regime release profile: initial, fast delivery of physically encapsulated molecules (t < 5 h) followed by slow release of the chemically bonded guests. This conclusion was in agreement with the SEM analysis of the particles during the dialysis process (Figure III-24). As previously observed for **M10**, **M9b** did not show appreciable degradation effects during the first 5 h, a period where guest delivery was mainly governed by diffusion. Surface erosion triggering degradation-induced release took place in a larger time scale and their effects were only visible after 26 h by SEM.

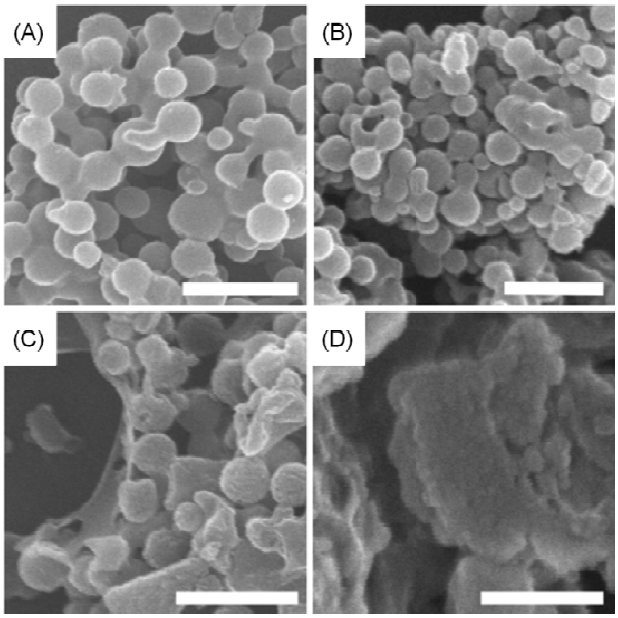

Figure III-24. SEM images of **M9b** CPPs suspended at 37 ºC in PBS for (a) 0 h, (b) 5 h, (c) 26 h and (d) 100 h. Scale bars are 500 nm.

III.2.4.2. Temperature dependent guest release from M9b and M10

After guest release experiments were carried out at physiological conditions, we wanted to exploit the valence tautomerism behavior exhibited by **M9b** and **M10** to thermally modulate their ability to deliver encapsulated substances. As pointed out before, the coordination polymers that constitute these two materials interconvert between two different electronic isomers when heated (see Figure III-18). Although such interconversion can also take place for the metal complex units of **M9b** where coordinating ligand **6** is chemically tethered, it should mostly affect the main polymer network of this material and **M10**, which is composed of cobalt ions and ligands **2** and **3** in both cases. Therefore, chemical and structural changes are expected to occur on these polymer matrices upon temperature increase, which should alter the kinetics of the diffusion and/or degradation mechanisms of release of the encapsulated guests. For instance, since larger Co-O and Co-N bonds are expected when switching from *ls*-Co(III) to *hs*-Co(II) states,[50] the porosity of the particles, and therefore, the diffusion coefficients of physically encapsulated guests through these materials may increase. Alternatively, changes in chemical stability arising from valence tautomerism may accelerate (or slow down) the erosion of **M9b** and **M10** in PBS, thus modulating degradation-induced delivery.

To investigate all these issues, guest release experiments were performed on **M9b** and **M10** at high temperature in PBS (60ºC) and the results obtained compared to those found at physiological conditions (i.e. 37ºC). It must be noted that the coordination polymers constituting these materials did not exist as pure electronic isomers at any of the two temperatures considered. Actually, based on the magnetic measurements shown in Figure III-18, the concentration ratio between *ls*-Co(III)

and *hs*-Co(II) states in **M9b** and **M10** was determined to be: (a) **M9b**: 1:4.5 at 37ºC and 1:3.1 at 60ºC; and (b) **M10**: 1:4 at 37ºC and 1:2.4 at 60ºC. In spite of this, we expected these changes in valence tautomer composition to be sufficient to yield significant changes in guest release kinetics at 37ºC and 60ºC.

Figure III-25A plots the cumulative guest release profiles determined at 60 ºC. Two main differences were observed with respect to the results obtained at 37ºC: (a) compounds **6** and **30** were delivered much faster from **M9b** and **M10** upon heating, with *ca*. 90% of these guests being released only in 3 h; for sake of comparison, such efficiency of release was only obtained after 100 h (**M9b**) and 9 h (**M10**) at 37ºC; and (b) while very different profiles were registered for **M9b** and **M10** at physiological conditions, the delivery kinetics measured for these materials were very similar, specially, when error bars were taken into account. These results indicate a dramatic thermal acceleration of the slowest release mechanism observed at 37ºC (i.e. degradation-induced delivery of guest molecules chemically tethered to the polymer network of **M9b**), which should become as fast as (or even faster than) diffusion of mechanically entrapped molecules and, eventually, control the release of both **6** and **30** molecules from **M9b** and **M10**.

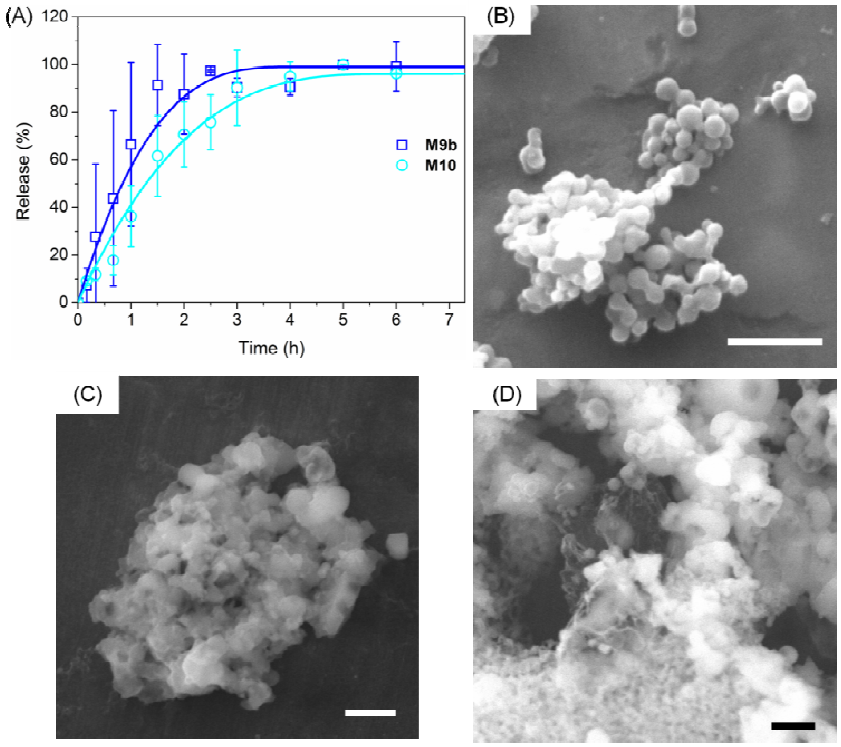

Figure III-25. (A) Guest release profiles of fluorescent molecules **6** and **30** from **M9b** and **M10** at 60 ºC, respectively, which were averaged over 3 independent experiments. Solid lines correspond to fits of the experimental data as described in the text. (B-D) SEM images of **M10** CPPs dialyzed at 60 ºC in PBS for (B) 0 h, (C) 3 h and (D) 6 h. Scale bars are 2 μm.

To demonstrate this hypothesis, two further actions were taken. First, **M9b** and **M10** release profiles were adjusted with Equation III-5, which accounts for single-mechanism degradation-induced delivery according to the Hopfenberg's model previously introduced. As shown in Figure III-24A, good agreement with the experimental data was achieved and very similar and high degradation rate constants were found for **M9b** ($k_d/C_0 = 3.27 \cdot 10^{-8}$ m s^{-1}) and **M10** ($k_d/C_0 = 8.05 \cdot 10^{-9}$ m s^{-1}). Second, the evolution in time of the morphology of the dialyzed particles was followed by SEM. Figure III-25B-D depict the microscopy images registered in these experiments for **M10**, which were equivalent to those acquired for **M9b**. Clearly, most nanoparticles lost their shape and size as fast as in just 3h of treatment in PBS at 60ºC, and they fully disintegrated and fused into larger continuous structures after 6 h. Since guest release completely took place in this period, this result further supported the conclusion that both physically and chemically encapsulated molecules in **M9b** and **M10** were mainly delivered via degradation processes at high temperatures, in contrast to the behavior observed at physiological conditions. We cannot currently tell whether this thermal effect arose from the valence tautomerism of the particles used or it was purely due to the increased rate of degradation in aqueous media expected for most CPPs upon heating. Nevertheless, our study clearly reveals that not only guest release kinetics but also the mechanism of delivery from these materials might be modulated by thermal stimuli.

$$M_t = M_\infty \cdot \left(1 - \left(1 - \frac{k_d t}{C_0 R}\right)^3\right) \qquad \text{(III-5)}$$

III.2.4.3. Exploiting our guest release models for drug delivery from CPPs

Once carefully investigated the different delivery mechanisms from Co-based CPPs doped with non-pharmacologically active fluorescent guests, we decided to go a step further and validate the release models developed in this work using as test systems other coordination polymer particles where real drugs were encapsulated via either chemical tethering or mechanical entrapment. In these studies, we mainly used Equation III-4 for release profile analysis, since it can account for any of the delivery mechanisms uncovered for **M9b** and **M10**: (a) purely diffusion-controlled release (if parameter b is set to 1); .(b) purely degradation-controlled release (if parameter b is set to 0); and (c) a combination of both mechanisms (if the value of b is not constrained and freely fitted).

As a case of chemical encapsulation, we focused our attention on the study of Huxford *et al.*[14] introduced above (see section 1.3.1.), where the authors investigated the release of an anticancer drug (MTX) coordinated to Gd-based CPPs. As such, drug delivery from this material was solely attributed to degradation processes. However, when fitting the delivery profile reported by them using Equation III-4 and b = 0 (i.e. assuming purely erosion-controlled release via a Hopfenberg's model), the experimental data could not be properly adjusted (Figure III-26). Similarly, negative

results were also obtained when attempting other fits with alternative single-mechanism degradation models. This situation largely resembled that encountered for **M9b**, which allowed us to uncover that a significant fraction of the coordinating guest molecules encapsulated were not chemically bonded but just physically trapped within the polymer network of the material. Accordingly, we fitted again the experimental results from Huxford *et al.*[14] with Equation III-4 but without predetermining the value of b (i.e. assuming that both erosion- and diffusion-controlled release mechanisms could take place). Surprisingly, a good agreement was found in this case with b = 0.9, k_D = 3.63·10^{-19} m^2 s^{-1} and k_d/C_0 = 8.52·10^{-14} m s^{-1} (Figure III-26). Therefore, these results indicate that only 10 % of the MTX molecules into the Gd-based CPPs prepared were covalently tethered, while the rest was mechanically entrapped within the material. Although this value might be overestimated due to the simplicity of our model (e.g. it does not consider variation of the diffusion coefficient as particle degradation proceeds), our treatment clearly demonstrates that care has to be taken when analyzing drug delivery from CPPs bearing chemically tethered therapeutic agents. For these systems, a fast diffusion-induced component in the release profile is to be expected corresponding to the fraction of the encapsulated molecules that lie mechanically trapped instead of covalently bonded to the materials, thus accelerating the overall drug delivery process. As a consequence, if CPPs with very slow drug release profiles are to be prepared, efforts must be focused on minimizing physical encapsulation of the active species.

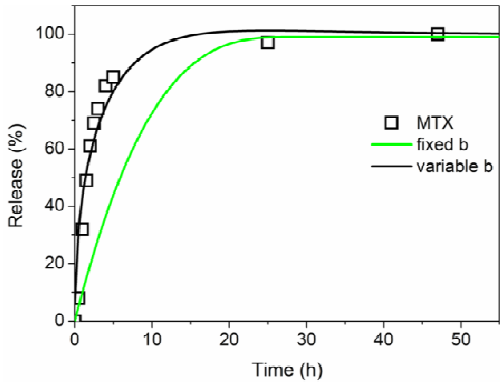

Figure III-26. Drug release profile of MTX from Gd-based CPPs reported by Huxford *et al.*[14] Solid lines correspond to fits of the experimental data as described in the text.

Next, we turned our attention to CPPs where drug molecules are physically encapsulated. In a first step, we decided to test the diffusion-controlled release model validated for **M10** in materials of similar composition and structure. With this aim, two new systems were developed in collaboration with Asli Raman and Dr. Fernando Novio from the group of Prof. Daniel Ruiz-Molina at the "Centre d'Investigació en Nanociència i Nanotecnologia (CIN2)". They were (i) Co-based CPPs (**M11**) and (ii) Fe-based CPPs (**M12**) bearing the fluorescent ,anticancer drug camptothecin **36** mechanically entrapped (Figure III-27A). The preparation of these nanoparticles was similar to that of **M10** and it was based on the use bisimidazole bridging linker **2** and *t*-butylcatechol **3** to coordinate the metal

ions of choice. In this case, however, fluorescent guest **30** was substituted by **36** and, for the synthesis of **M12**, an iron metal precursor ($Fe(OAc)_2$) was added to the mixture of organic ligands instead of cobalt(II) acetate. In this way, camptothecin-doped coordination polymer particles of different metal ions and analogous to **M10** were synthesized, with which drug encapsulation efficiencies of 25 % (**M11**) and 27 % (**M12**) were achieved. Drug release experiments on the new materials were done at physiological conditions as previously explained for **M9b** and **M10**. Both materials showed a similar behavior to that found for **M10** and almost all the amount of encapsulated drug was released after 10 hours. More importantly, when fitting the release profiles measured with Equation III-4 and b=1, a good agreement was found with the experimenta data. Therefore, in agreement to **M10**, drug release from new materials **M11** and **M12** could be fully justified on the basis of a single diffusion-controlled mechanism of release. The apparent diffusion constants retrieved from the fit were k_D = $4.59 \cdot 10^{-19}$ and $6.97 \cdot 10^{-19}$ m^2 s^{-1} for **M11** and **M12**, respectively, which indicated that the structure of these materials and, therefore, the kinetics of diffusion of camptothecin molecules though them had to be similar.

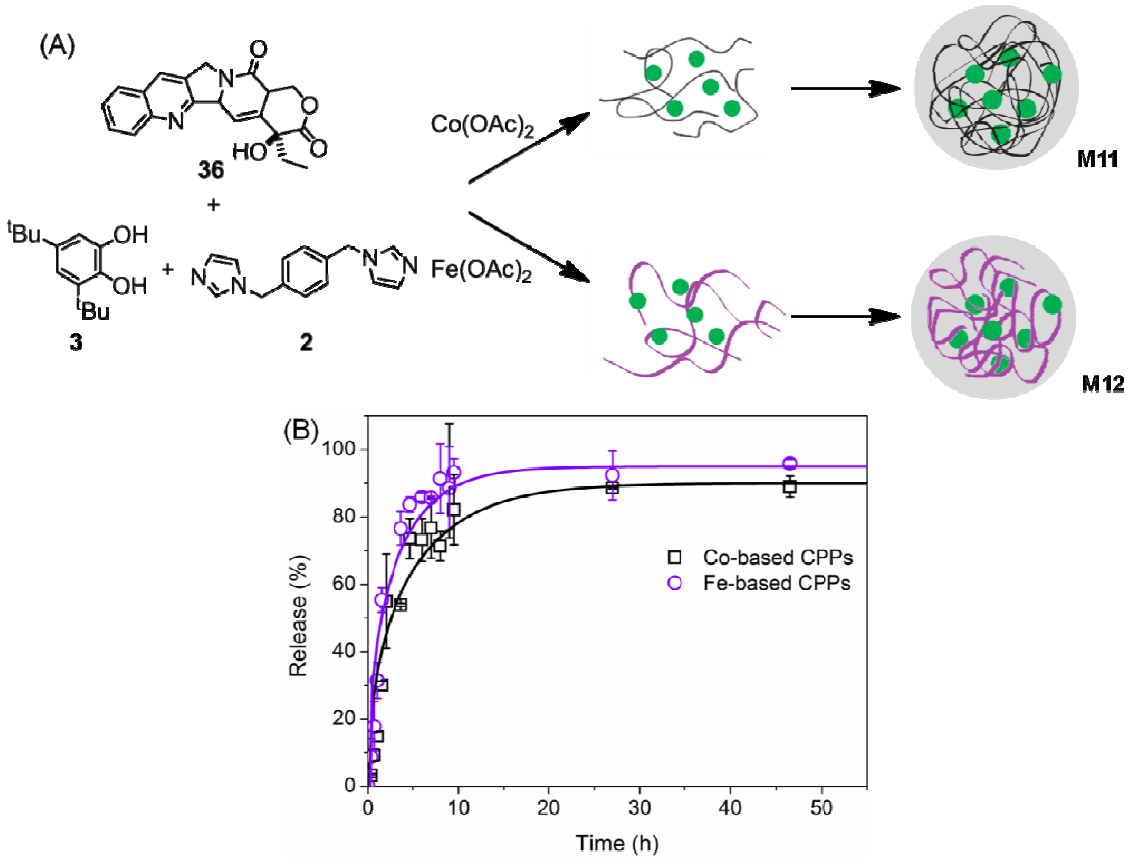

Figure III-27. (A) Schematic representation of the camptothecin (**36**) encapsulation within Co- and Fe-based CPPs. (B) Drug release profiles of **35** from **M11** and **M12** at 37 ºC, which were averaged over 3 independent experiments. Solid lines correspond to fits of the experimental data as described in the text.

III.3. CONCLUSIONS

This chapter reported the preparation of Co-based CPPs doped with fluorescent molecules for investigating the mechanisms of guest encapsulation and release from coordination polymer particles. With this aim, the following experiments were performed:

1. Different model fluorescent guests were synthesized and characterized, which consisted in dyads of a benzophenoxazine dye and a *t*-butylcatechol unit with unprotected (**4**, **5**, **6**) or protected hydroxyl groups (**30**). All of them were prepared from commercial 2-methoxy-4-methylphenol: (a) **4**: in 10 steps and 0.5 % yield; (b) **5** and **6**: in 9 steps and 3 % yield, and (c) **30** in 8 steps and 2 % yield. Based on its higher synthetic yield and better optical properties, compound **6** bearing a chelating catechol ligand was chosen for the preparation of Co-based CPPs via coordination to the metal ions of the system. Catechol-protected, non-coordinating compound **30** was then designed to carry the same benzophenoxazine dye and used for the preparation of analogous particles where the fluorescent guests were physically encapsulated instead of chemically bonded.

2. Co-based CPPs bearing compounds **6** (**M9b**) and **30** (**M10**) were synthesized according to the literature[15], using a bisimidazole ditopic linker for the formation of the coordination polymers and *t*-butylcatechol groups to saturate the coordination sphere of the cobalt ions. Care had to be taken to properly select the concentration of guests **6** and **30** to be used in the preparation of these materials, since we demonstrated that the addition of higher amounts (> 1 mM) of these compounds led to self-structuration into microparticles driven by π-stacking of their benzophenoxazine groups. Consequently, **M9b** and **M10** were prepared with low doping content of **6** (2.1 % wt.) and **30** (1.1 % wt.), the encapsulation efficiencies measured being higher for the former compound given the coordinating capacity of its unprotected catechol group. Such low guest concentrations resulted in very similar morphological and structural features for both materials (average diameter ~ 170 nm), which displayed the same valence tautomer behavior as analogous undoped particles. Thus, we observed that the metal complex units of their constituent coordination polymers converted from *ls*-Co(III) to *hs*-Co(II) states upon temperature increase, as revealed by magnetic experiments. Finally, fluorescence measurements were used to reveal that the emission from **6** and **30** was quenched when encapsulated within **M9b** and **M10**, respectively, thereby allowing selective detection of free, delivered guests in our subsequent release studies.

3. Guest release experiments were conducted for Co-based CPPs **M9b** and **M10**. While no significant differences were observed at high temperatures (i.e. 60ºC), clearly different delivery profiles were measured for the two systems at physiological conditions. We could interpret these results on the basis of distinct encapsulation and release mechanisms according to mathematical models developed for drug release from organic polymeric materials and SEM analysis of the evolution of the particles. Thus, delivery of mechanically entrapped guest **30** from **M10** was

encountered to be mainly associated to fast diffusion processes through the material at 37ºC, which took place in a shorter time scale than slow particle degradation at this temperature. In case of **M9b**, our analytical treatment revealed the occurrence of two different populations of encapsulated guests, physically trapped and chemically bonded molecules. As such, its release profile showed two different regimes at physiological conditions, which resulted from the separate delivery of each one of those populations via fast degradation and slow diffusion processes, respectively. Upon heating, however, degradation of the particles was found to be enormously accelerated and it became the major release mechanism for both **M9b** and **M10**. To account for all these possibilities (i.e. diffusion-controlled release, degradation-controlled release or combination of both), a new mathematical model for drug delivery analysis was derived (Equation III-4), whose general applicability was successfully validated using as test systems different drug-loaded CPPs from the literature as well as specifically prepared in this work.

In conclusion, we have demonstrated in this chapter that drug delivery kinetics from CPPs can be easily modulated by proper choice of the encapsulation mechanism of therapeutic agents. Thus, by cleverly combining fast diffusion of mechanically entrapped molecules together with slow degradation-controlled release of chemically bonded guests, the delivery profiles from these materials can be finely tuned and adjusted on demand to the time window of action of the target drugs.

III.4. REFERENCES

[1] A. M. Spokoyny, D. Kim, A. Sumrein, C. A. Mirkin, *Chem. Soc. Rev.* **2009**, *38*, 1218-1227.

[2] (a) B. F. Hoskins, R. Robson, *J. Am. Chem. Soc.* **1990**, *112*, 1546‑1554. (b) J. S. Seo, D. Whang, H. Lee, S. I. Jun, J. Oh, Y. J. Jeon, K. Kim, *Nature* **2000**, *404*, 982‑986. (c) H. Liu, Y. Liu, Y. Li, Z. Tang, H. Jiang, *J. Phys. Chem. C* **2010**, *114*, 13362‑13369.

[3] (a) A. P. Nelson, O. K. Farha, K. L. Mulfort, J. T. Hupp, *J. Am. Chem. Soc.* **2009**, *131*, 458‑460. (b) L. Ma, A. Jin, Z. Xie, W. Lin, *Angew. Chem., Int. Ed.* **2009**, *48*, 9905‑9908. (c) Z. Wang, K. K. Tanabe, S. M. Cohen, *Chem. Eur. J.* **2010**, *16*, 212‑217. (d) P. D. C. Dietzel, Y. Morita, R. Blom, H. Fjellvag, *Ang. Chem. Int. Ed.* **2005**, *44*, 6358-6362.

[4] (a) G. Férey, C. Mellot-Draznieks, C. Serre, F. Millange, J. Dutour, S. Surblé, I. Margiolaki, *Science* **2005**, *310*, 2040-2042. (b) F. Ke, Y-P. Yuan, L-G. Qiu, Y-H. Shen, A-J. Xie, J-F. Zhu, X-Y Tian, L-D. Zhang, *J. Mater. Chem.* **2011**, *21*, 3843-3848.

[5] (a) M. Oh, C. A. Mirkin, *Angew. Chem. Int. Ed.* **2006**, *45*, 5492-5494. (b) S. Jung, M. Oh, *Angew. Chem. Int. Ed.* **2008**, *47*, 2049-2051. (c) W. Lu, S. S-Y. Chui, K-M. Ng, C-M. Che, *Angew. Chem. Int. Ed.* **2008**, *47*, 4568-4572. (d) W. J. Rieter, K. M. L. Taylor, H. An, W. Lin, W. Lin, *J. Am. Chem. Soc.* **2006**, *128*, 9024-9025.

[6] F. Novio, J. Simmchen, N. Vázquez-Mera, L. Amorín-Ferré, D. Ruiz-Molina, *Coord. Chem. Rev.* **2013**, *257*, 2839-2847.

[7] M. Oh, C.A. Mirkin, *Nature* **2005**, *438*, 651-654.

[8] D. Tanaka, A. Henke, K. Albrecht, M. Moeller, K. Nakagawa, S. Kitagawa, J. Groll, *Nat. Chem.* **2010**, *2*, 410-416.

[9] L-N. Jin, Q. Liu, Y. Yang, H-G. Fu, W-Y. Sun, *J. Coll. Inter. Sci.* **2014**, *426*, 1-8.

[10] Y-M. Jeon, G. S. Armatas, D. Kim, M. G. Kanatzidis, C. A. Mirkin, *Small* **2009**, *5*, 46-50.

[11] X. Sun, S. Dong, E. Wang, *J. Am. Chem. Soc.* **2005**, *127*, 13102-13103.

[12] H. Wei, B. Li, Y. Du, S. Dong, E. Wang, *Chem. Mater.* **2007**, *19*, 2987-2993.

[13] R. Nishiyabu, N. Hashimoto, T. Cho, K. Watanabe, T. Yasunaga, A. Endo, K. Kaneko, T. Niidome, M. Murata, C. Adachi, Y. Katayama, M. Hashizume, N. Kimizuka, *J. Am. Chem. Soc.* **2009**, *131*, 2151-2158.

[14] R. C. Huxford, K. E. de Krafft, W. S. Boyle, D. Liu, W. Lin, *Chem. Sci.* **2012**, *3*, 198-204.

[15] I. Imaz, D. Maspock, C. Rodríguez-Blanco, J. M. Pérez-Falcón, J. Campo, D. Ruiz-Molina, *Angew. Chem. Int. Ed.* **2008**, *47*, 1857-1860.

[16] (a) Y. Lou, Y. Tao, J. Wang, J. Chen, M. Ohba, *Polyhedron* **2014**, *73*, 72-76. (b) Z-B. Han, J-W. Ji, H-Y. An, W. Zhang, G-X. Han, G-X. Zhang, L-G. Yang, *Dalton Trans.* **2009**, 9807-9811.

[17] D. M. Adams, D. N. Hendrickson, *J. Am. Chem. Soc.* **1996**, *118*, 11515-11528.

[18] (a) E. Evangelio, D. Ruiz-Molina, *Eur. J. Inorg. Chem.* **2005**, 2957-2971. (b) D. M. Adams, A. Dei, A. L. Rheingold, D. N. Hendrikson, *J. Am. Chem. Soc.* **1993**, *115*, 8221-8229. (c) D. Ruiz-Molina, J. Yoo, I. A. Guzei, A. L. Rheingold, D. N. Hendrickson, *Chem. Commun.* **1998**, 2089-2090. (d) N. G. R. Hearns, J. L. Korcok, M. M. Paquette, K. E. Preuss, *Inorg. Chem.* **2006**, *45*, 8817-8819.

[19] I. Imaz, J. Hernando, D. Ruiz-Molina, D. Maspoch, *Angew. Chem. Int. Ed.* **2009**, *48*, 2325-2329.

[20] O. K. Farha, A. M. Spokoyny, K. L. Mulfort, J. T. Hupp, C. A. Mirkin, *Small* **2009**, *5*, 1727-1731.

[21] Y-M. Jeon, J. Heo, C. A. Mirkin, *J. Am. Chem. Soc.* **2007**, *129*, 7480-7481.

[22] K. H. Park, K. Jang, S. U. Son, D. A. Sweigart, *J. Am. Chem. Soc.* **2006**, *128*, 8740-8741.

[23] (a) Y-M. Jeon, G. S. Armatas, J. Heo, M. G. Kanatzidis, C. A. Mirkin, *Adv. Mater.* **2008**, *20*, 2105-2110. (b) Y. Sun, H. Yu, L. Wang, Y. Zhao, W. Ding, J. Ji, Y. Chen, F. Ren, Z. Tian, L. Huang, P. Ren, R. Tong, *J. Inorg. Organomet. Polym.* **2014**, *24*, 491-500. (c) K. Wang, X. Ma, D. Shao, Z. Geng, Z. Zhang, Z. Wang, *Cryst. Growth Des.* **2012**, *12,* 3786-3791.

[24] (a) W. J. Rieter, J. S. Kim, K. M. L. Taylor, H. An, W. Lin, T. Tarrant, W. Lin, *Angew. Chem. Int. Ed.* **2007**, *46*, 3680-3682. (b) J. Wu, Z. Ye, G. Wang, D. Jin, J. Yuna, Y. Guan, J. Piper, *J. Mater. Chem.* **2009**, *19*, 1258-1264.

[25] (a) L. Kelland, *Nat. Rev. Cancer* **2007**, *7*, 573-584. (b) E.A. Flügel, A. Ranft, F. Haase, B.V. Lotsch, *J. Mater. Chem.* **2012**, *22*, 10119-10133. (c) L. Xing, Y. Cao, S. Che, *Chem. Commun.* **2012**, *48*, 5995-5997. (d) W. J. Rieter, K. M. Pott, K. M. L. Taylor, W. Lin, *J. Am. Chem. Soc.* **2008**, *130*, 11584-11585. (e) I. Imaz, M. Rubio-Martínez, L. García-Fernández, F. García, D. Ruiz-Molina, J. Hernando, V. Puntes, D. Maspoch, *Chem .Commun.* **2010**, *46*, 4737-4739. (f) P. Huang, J. Mao, L. Yang, P. Yu, L. Mao, *Chem. Eur. J.* **2011**, *17*, 11390-11393.

[26] (a) J. Yang, W. Liu, M. Sui, J. Tang, Y. Shen, *Biomaterials*, **2011**, *32*, 9136-9143. (b) L. Xing, Y. Cao, S. Che, *Chem. Commun.*, **2012**, *48*, 5995-5997. (c) R. C. Huxford, K. E. de Krafft, W. S. Boyle, D. Liu, W. Lin, *Chem. Sci.*, **2012**, *3*, 198-204.

[27] L. Xing, H. Zheng, S. Che, *Chem. Eur. J.* **2011**, *17*, 7271-7275.

[28] (a) Basché, T.; Moerner, W. E.; Orrit, M.; Wild, U. P. *Single-molecule Optical Detection, Imaging and spectroscopy*. VCH: Berlin, Germany, **1996**. (b) Moerner, W. E.; Orrit, M. Science. **1999**, 283, 1670-1676.

[29] J. R. Lakowicz, *Principles of fluorescence spectroscopy*. Kluwer Academic: New York, **1999**.

[30] Q. Wang, Y. Yang, Y. Li, W. Yu, Z. J. Hou, *Tetrahedron* **2006**, *62*, 6107-6112.

[31] G. Bringmann, T. Pabst, P. Henschel, J. Kraus, K. Peters, E-M. Peters, D. S. Tycroft, J. D. Connolly, *J. Am. Chem. Soc.* **2000**, *122*, 9127-9133.

[32] P. J. Kocienski, *Protecting groups* (3rd Ed.). Thieme: Stuttgard, **2003**.

[33] D. A. Shultz, M. G. Hollomon, *Chem. Mater.* **2000**, *12*, 580-585.

[34] E. Pretsch, P. Bühlmann, M. Badertscher, *Structure determination of organic compounds* (4th Ed.). Springer: New York, **2009**.

[35] F. A. Carey, R. J. Sundberg, *Advanced Organic Chemistry*, *Part C: Reactions and Synthesis* (4th Ed.). Springer science + Business media: New York, **2000**.

[36] W. Ngeontae, C. Xu, N. Ye, K. Wygladacz, W. Aeungmaitrepirom, T. Tuntulani, E. Bakker, *Anal. Chim. Acta* **2007**, *599*, 124-133.

[37] M. Dudic, P. Lhoták, I. Stibor, K. Lang, P. Prosková, *Org. Lett.* **2003**, *5*, 149-152.

[38] V. H. J. Frade, M. S. T. Gonçalves, P. J. G. Coutinho, J. C. V. P. Moura. *Photochem. Photobiol. A* **2007**, *185*, 220-230.

[39] S. A. Martin-Brown, Y. Fu, G. Saroja, M. M. Collinson, D. A. Higgins, *Anal. Chem.* **2005**, *77*, 486-494.

[40] V. H. J. Frade, M. S. T. Gonçalves, P. J. G. Coutinho, J. C. V. P. Moura. *J. Photochem. Photobiol. A* **2007**, *185*, 220-230.

[41] (a) M. L. Crossley, R. J. Turner, C. M. Hofman, P. F. Dreisbach, R. P. Parker, *J. Am. Chem. Soc.* **1952**, *74*, 578-584.

[42] R. Sens, K. H. Drexhage, *J. Luminesc.* **1981**, *24,* 709-712.

[43] P. K. Dhal, F. H. Arnold, *Macromolecules* **1992**, *25*, 7051-7059.

[44] D. M. Adams, L. Noodleman, D. N. Hendrickson, *Inorg. Chem.* **1997**, *36*, 3966-3984.

[45] N. V. Anh, R. M. Williams, *Photochem. Photobiol. Sci.*, **2012**, *11*, 957-961.

[46] (a) J. Crank, *The Mathematics of Diffusion*, (Clarendon Press), Oxford, **1975**. (b) J. Siepmann, F. Siepmann, *Int. J. Pharm.*, **2011**, *418*, 42-53.

[47] H. B. Hopfenberg, in *Controlled Release Polymeric Formulations*, Vol 33 (Eds: D. R. Paul, F. W. Harris), ACS symposium Series 33, American Chemical Society, Washington, **1976**.

[48] (a) Z. Ramtoola, O. I. Corrigan, C. J. Barrett, *J. Microencap.*, **1992**, *9*, 415-423. (b) C. K. Sackett, B. Narasimhan, *Int. J. Pharm.* **2011**, *418*, 104-114.

[49] P Costa, J. M. Sousa, *Eur. J. Pharm. Sci*. **2001**, *13*, 123-133.

[50] O-S. Jung, C. G. Pierpont, *Inorg. Chem.* **1994**, *33*, 2277-2235.